

Mononuclear palladium(I) and palladium(III) coordination compounds

Siddhartha Banerjee¹, Sagnik Chakrabarti¹, Bailey S. Bouley, Amy J. Wahlmeier, Liviu M. Mirica^{*}

Department of Chemistry, University of Illinois Urbana-Champaign, Urbana, IL 61801, USA

ARTICLE INFO

Keywords:

Palladium(I)
Palladium(III)
Metalloradical
Paramagnetic
Electron paramagnetic resonance (EPR)
Mononuclear
Intermediates
X-ray crystallography

ABSTRACT

Palladium coordination complexes are invaluable catalysts in organometallic reactions, facilitating a plethora of synthetically useful organic transformations that include C–H functionalization and C–C/C–heteroatom bond formation reactions. The proposed mechanisms for such reactions usually invoke two-electron pathways involving diamagnetic Pd⁰, Pd^{II}, and Pd^{IV} intermediates. However, recent research has focused on the viability of paramagnetic Pd species with +1 and +3 oxidation states as plausible intermediates. The past two decades have seen a renewed interest in the isolation and characterization of such transient species to obtain a better understanding of their structure and reactivity. This review focuses on the coordination chemistry of mononuclear Pd^I and Pd^{III} compounds that have been isolated and characterized using spectroscopic techniques such as electron paramagnetic resonance (EPR), nuclear magnetic resonance (NMR), cyclic voltammetry (CV), electrospray ionization mass spectrometry (ESI-MS), single crystal X-ray crystallography (SC-XRD), and X-ray absorption spectroscopy (XAS) methods. It is expected that the knowledge gained from studying the electronic structure and spectroscopic properties of these compounds will be used to facilitate new modes of reactivity inaccessible to traditional Pd^{0/II/IV} chemistry.

1. Introduction

Palladium is the most privileged transition metal in homogeneous catalysis, given the widespread use of its coordination compounds as catalysts for C–H functionalization and cross-coupling reactions. It is virtually synonymous with metal-catalyzed cross-coupling reactions, as demonstrated by the Nobel Prize in Chemistry in 2010 being awarded to Heck, Negishi, and Suzuki for pioneering the development of such Pd-catalyzed chemical transformations [1]. The commonly accepted mechanism of these reactions, usually involving the coupling of an aryl halide (or pseudohalide) with an aryl organometallic fragment, have been established to go through closed-shell, diamagnetic intermediates such as Pd⁰ and Pd^{II} species. The detailed mechanistic understanding of the reaction mechanisms has led to the development of many examples of Pd-catalyzed bond-forming reactions besides the aforementioned, such as Kumada, Buchwald-Hartwig, Sonogashira, Hiyama, and Stille couplings [2]. The vast majority of these reactions proceed via the following mechanistic steps: 1) oxidative addition of an aryl halide (ArX) into a Pd⁰ species to generate a Pd^{II}(Ar)X intermediate; 2) transmetalation of a nucleophilic coupling partner (the identity of which

often determines the type of reaction) to generate the bis-organometallic Pd^{II}(Ar¹)(Ar²); 3) reductive elimination of the aryl groups to form the cross-coupled Ar¹-Ar² species and regenerate the active Pd⁰ catalyst, which completes the catalytic cycle (Fig. 1). In recent years, significant strides have also been made in using Pd catalysts for facilitating C–H functionalization reactions [3,4] and the proposed mechanisms often invoke high-valent diamagnetic states, usually operating via Pd^{II}/Pd^{IV} cycles [5].

The choice of Pd as the transition metal catalyst for these reactions is largely dictated by the accessibility and highly predictable reactivity of coordination complexes of Pd⁰ and Pd^{II} states. This facilitates the rational development of new catalysts by ligand design and allows the systematic study of their reactivity. However, there are significant downsides of Pd catalysis when it comes to building molecular three-dimensional complexity. Pd-based systems often fail in cases where alkyl substrates are used as coupling partners. This is due to the high barrier of the oxidative addition step in the case of alkyl electrophiles, [6] or the propensity of Pd-alkyl organometallic fragments to undergo β-hydride elimination, owing to the high d-orbital diffusivity of Pd, [7,8] and thus resulting in significant side reactivity. Interestingly, nickel (Ni)

^{*} Corresponding author.

E-mail address: mirica@illinois.edu (L.M. Mirica).

¹ These authors contributed equally.

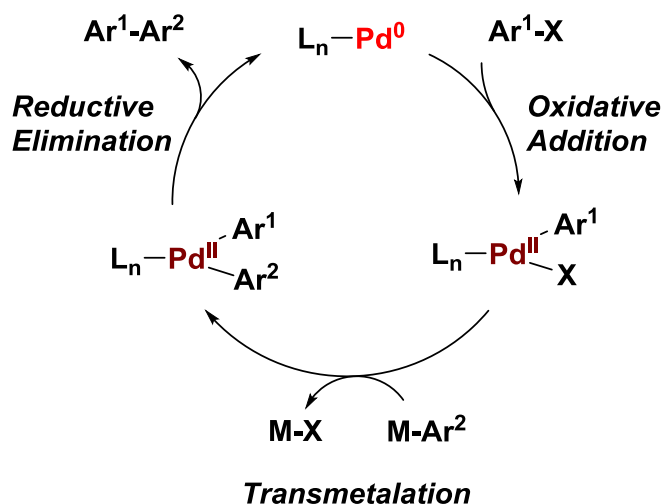


Fig. 1. General catalytic cycle for Pd-catalyzed C–C cross-coupling reactions.

the lighter congener of Pd, has proven to be competent in performing reactions that are typically challenging for Pd, such as alkyl-alkyl cross couplings [9,10]. As a first-row metal, Ni has significantly constricted d orbitals relative to Pd, decreasing rates of β -hydride elimination [11]. Additionally, the ability of Ni to access the less-common “odd” oxidation states of Ni^I and Ni^{III} can result in radical reactivity, leading to the activation of unreactive alkyl halide substrates and cross coupling reactions occurring via a catalytic cycles that involve single-electron steps, rather than the more common two-electron chemistry shown in Fig. 1 [12,13].

The existence of stable and isolable mononuclear Ni^I and Ni^{III} compounds that demonstrate unique reactivity begets the question of whether such compounds exist for Pd and if they may allow the reactivity that has been traditionally elusive for Pd. To examine this, it is worth looking at the electronic structure of Pd^{III} and Pd^I coordination compounds. Pd^{III} compounds, which are d⁷ ions, will be expected to prefer a Jahn-Teller distorted octahedral geometry with the unpaired electron expected to be in the d_{z²} orbital (Fig. 2a) [14,15]. Pd^I compounds, on the other hand, would feature a d⁹ electronic configuration and would favor square-based or lower coordinate geometries with an unpaired electron located in the d_{x²-y²} orbital (Fig. 2b) [16]. The existence of a metalloradical implies that the most thermodynamically favorable configuration for these compounds would be the formation closed-shell diamagnetic compounds with a metal-metal bond. This is in fact the case, and the chemistry of Pd^I and Pd^{III} compounds have been

dominated by dimeric compounds featuring Pd–Pd bonds. These dimeric systems have found their own niche in chemical transformations. For example, the Ritter group reported in 2009 the use of Pd^{III} dimers for directed C–H functionalization to generate C–Cl and C–O bonds catalytically [14,17]. On the other hand, Pd^I dimers as catalysts have undergone a renaissance over the last 20 years, especially the phosphine-ligated [(PR₃)Pd^I(μ -X)]₂ dimers synthesized by Mingos and popularized by the Hartwig group initially [18] and later by Schoenebeck, Colacot, and others [19,20]. Their use has gained traction in many cross-coupling reactions, as well as some bimetallic catalysis (Fig. 3). The rich chemistry of dinuclear Pd^I and Pd^{III} compounds have been reviewed elsewhere and will not be the subject of discussion of the present review [19,21].

Isolated, mononuclear Pd^I and Pd^{III} compounds are significantly rarer, and examples of such coordination complexes have only begun to emerge in the last two decades. While they have been proposed as reaction intermediates in chemical transformations, the difficulty in isolating such compounds means that their electronic structure and stoichiometric reactivity remain poorly understood. The possible role of paramagnetic Pd^I compounds as reaction intermediates in the photo-catalyzed radical activation of alkyl iodides have been reported as far back as 1995 by Suzuki and Miyaura [25]. Several recent reports have revitalized this mode of reactivity as an attractive complementary tool to the traditional two-electron oxidative addition pathway and allow the activation of electrophiles that are traditionally inaccessible to ground-state Pd catalysis [26–36].

Mononuclear Pd^{III} intermediates have been proposed to be involved in oxidation-induced reductive coupling reactions from Pd^{II}-alkyl or -aryl species from the groups of Milstein [37] and Sanford [38]. There is some evidence that Pd^{III} intermediates are involved in isopropyl iodide-enhanced Kumada cross coupling reactions and some oxygen-mediated C–O bond forming reactions [39,40]. Recently, our group and others have devised strategies that allow for the isolation and characterization of these species to probe their roles in reactivity. This review outlines the progress that has been made in understanding the coordination chemistry and reactivity of such mononuclear Pd^I and Pd^{III} compounds.

2. Mononuclear palladium(I) compounds

2.1. Palladium(I) compounds stabilized by monodentate phosphine ligands

The first mononuclear Pd^I compounds were reported concurrently by the Chaplin and Ozerov groups. Chaplin and coworkers reported the first example of an unsupported two-coordinate Pd^I complex, **2a** (Fig. 4) [41]. This was achieved via the one-electron oxidation of a widely used

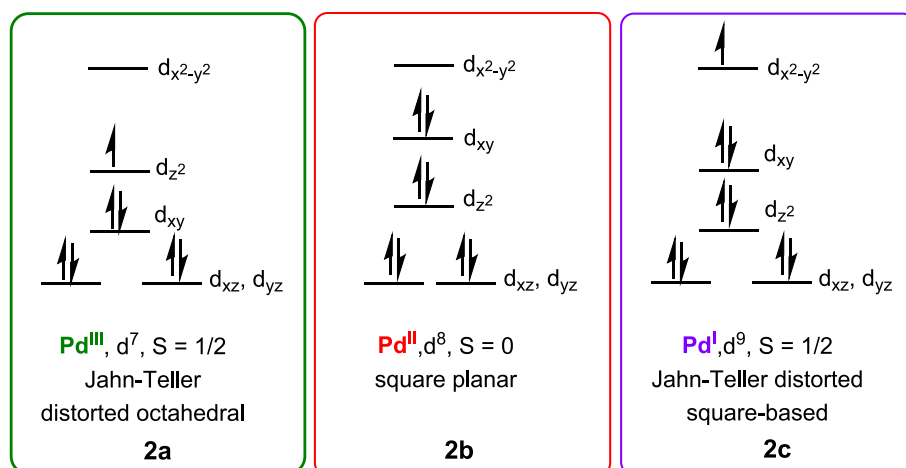


Fig. 2. Simplified illustration of d electron configurations of Pd in the +3, +2, and +1 oxidation states.

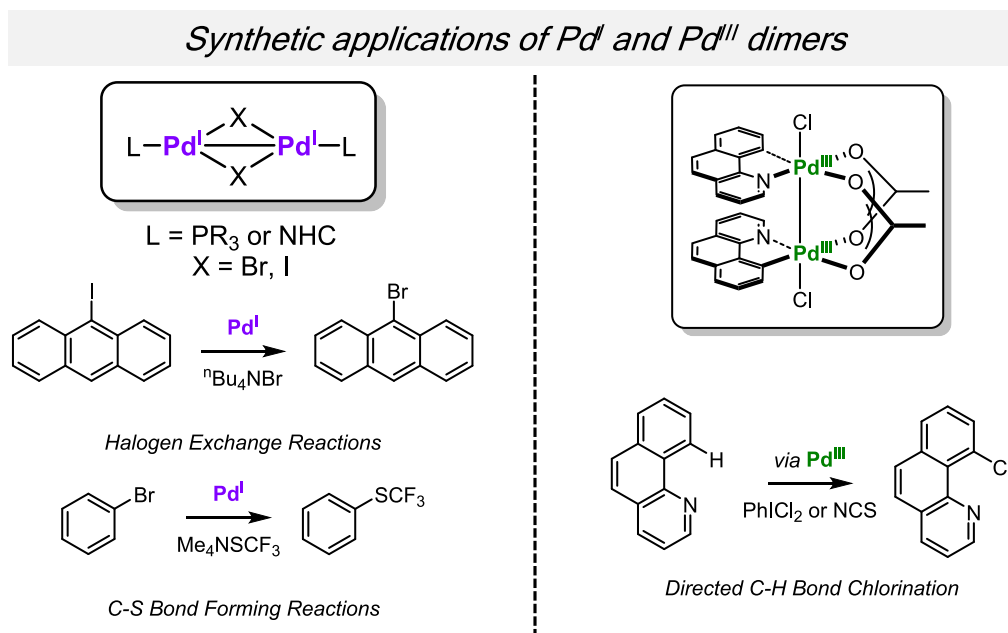


Fig. 3. Selected examples of reactions catalyzed by dinuclear Pd^I and Pd^{III} compounds [22–24].

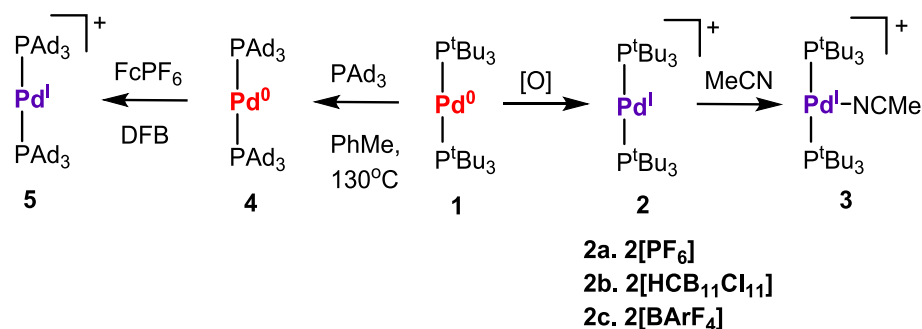


Fig. 4. Syntheses of mononuclear Pd^I complexes supported by monodentate phosphine P^tBu₃. [O] refers to the oxidant employed, which are ferrocenium hexafluorophosphate (FcPF₆), trityl cation supported by the chloride derivative of monocarba-*closo*-dodecaborate ([Ph₃C][HCB₁₁Cl₁₁]), and ferrocenium tetrakis[3,5-bis(trifluoromethyl)phenyl]borate (FcBAR₄) for **2a**, **2b**, and **2c**, respectively.

Pd⁰ complex, [Pd⁰(P^tBu₃)₂] (**1**) [42,43]. In the same year, Ozerov and coworkers used the same complex to synthesize **2b** [44]. Cyclic voltammetry studies in 1,2-difluorobenzene (DFB) for **1** revealed quasi-reversible peaks, [45] prompting the authors to react **1** with [Fc][PF₆] and [Ph₃C][HCB₁₁Cl₁₁] to generate the blue-colored [Pd^I(P^tBu₃)₂][PF₆] (**2a**) and [Pd^I(P^tBu₃)₂][HCB₁₁Cl₁₁] (**2b**), respectively (Fig. 4).

During the synthesis of **2b**, the ¹H NMR spectrum of the reaction mixture showed the formation of Gomberg's dimer, which was generated by the dimerization of trityl radicals [46]. Both complexes were highly symmetrical with the Pd atom at the center of inversion, and more elongated M-P bonds than the corresponding neutral complex. Although both **2a** and **2b** were air-sensitive in solution, they showed good stability under argon. Moreover, **2b** had a magnetic moment of 1.5 μ_B, consistent with one unpaired electron of a d⁹ Pd^I, and underwent reversible coordination with MeCN to form **3**. The EPR spectrum for **2** at 200 K showed an isotropic signal centered at g = 2.3 along with strong hyperfine coupling to ¹⁰⁵Pd, confirming the presence of an S = 1/2 Pd^I species. The room temperature EPR spectrum for the acetonitrile adduct **3** showed an isotropic signal at g = 2.172, with significantly lower hyperfine coupling, suggesting substantial electron delocalization from the metal center onto the ligands. The Ozerov group performed density functional theory (DFT) calculations to interpret the unusually elongated M-P bonds in the cationic Pd^I species. It was revealed that the

observed increase in the M-P distance in the oxidized partner is due to the removal of an electron from the molecular orbital (MO) involved in M → PR₃ π-backbonding. This led to a weaker M-P interaction, ultimately resulting in a longer M-P distance [47,48].

An alternative deduction makes use of Bent's rule, which states that when a metal oxidizes, more electronegative groups are linked to P, causing the M-P σ-bond to have more p-character and the PR₃ σ-bonds to have more s-character. This causes the M-P bond to lengthen [49–55]. In 2023, the same group explored C–H activation with the Pd^I metalloradical **2**; this time, the weakly coordinating counteranion [BAR₄^F][−] (Ar^F = 3,5-(CF₃)₂C₆H₃) was used, which showed similar EPR signals to **2a** and **2b** [56]. The crystal structure, however, featured a disordered mixture of staggered and eclipsed cations in equal ratios. To investigate the donor strength of phosphine ligands, the corresponding Pd⁰(PAd₃)₂ complex **4** was synthesized; [57] one electron oxidation of **4** by [Fc][BAR₄^F] led to the formation of **5** in >80 % yields, as confirmed by EPR, which indicated the presence of a metalloradical signal with a sextet pattern arising from isotropic hyperfine coupling to ¹⁰⁵Pd. Moreover, X-ray diffraction studies for **5** revealed well-ordered and linear geometry for the complex.

Since oxidative addition is a key elementary step in Pd-catalyzed cross-coupling reactions, [58,59] Chaplin and coworkers investigated alkyl and aryl iodide activation by this [Pd^I(P^tBu₃)₂] metalloradical

[60]. **2** was subjected to reaction with phenyl iodide in DFB to generate a 1:2 mixture of Pd^I iodide dimer **6** and a phenyl phosphonium salt (Fig. 5). The addition of excess phenyl iodide, tracked by UV-vis and NMR spectroscopy indicated complete consumption of the Pd^I complex and formation of a diamagnetic Pd^{II} aryl intermediate. Electron-donating methoxy-substituted aryl iodides were selected as ideal candidates to crystallize the Pd^{II} oxidative addition complexes. Reactions of [Pd^I(P^tBu₃)₂] with 2-methoxy and 2,6-dimethoxy-phenyl iodide lead to the formation of persistent Pd^{II} aryls, [Pd(P^tBu₃)₂Ar][PF₆] [Ar = 2-(MeO)C₆H₄, **7**; 2,6-(MeO)₂C₆H₃, **8**] albeit in modest yields (up to 38 %). Adamantyl and tert-butyl iodide were also tested to expand the reaction scope; whereas the former resulted in the formation of **6** and [P^tBu₃Ad][PF₆], in the latter case the Pd^{II}-alkyl complex underwent rapid β-hydrogen elimination.

Chaplin and coworkers provided NMR evidence that complex **2** could be treated with a base (2,6-bis(decyl)pyridine) to form cyclo-metalated Pd^{II} complex **9** [41]. In an independent report, they synthesized **9** and oxidized it with excess iodosobenzene (PhIO) to form the ring-expansion product **10** [61]. Both complexes were distorted T-shaped with a marked reduction in Pd–C bond length and reduction in ring strain upon moving from the 4-membered to the 5-membered ring. In the same report, the authors mentioned that they serendipitously discovered that both **9** and **10** could be generated by the aerobic oxidation of **2** in DFB.

In 2018, Chaplin and Hooper showed that **2** could be used in the oxidative cross-coupling of aryl trifluoroborates and aryl-antimony reagents to form the corresponding cross-coupled product [62]. This coupling was proposed to be mediated via a Pd^IPd^I–Pd^{II}Pd^{II}–Pd⁰Pd⁰ bimetallic fashion, with ferrocenium as an oxidant to regenerate the metalloradical, proving that isolated mononuclear Pd^I complexes are catalytically competent, albeit requiring external oxidants and two metal centers to perform the chemistry. Both the independently synthesized and the in situ generated Pd^I complex tolerated a variety of substrates, with more than 20:1 selectivity for cross-coupled products.

2.2. Palladium(I) compounds stabilized by thiapyridinophane ligands

In 2020 the Mirica group reported a series of transient Pd^I complexes supported by the ^tBuN₄ (*N*, *N'*-di-tert-butyl-2,11-diaza[3.3](2,6)

pyridinophane) [63] and N2S2 (2,11-dithia[3.3](2,6)pyridinophane) [64] pyridinophane ligands [65]. The influence of a variety of auxiliary ligands were explored, including nitriles, isonitriles, methyl, halides, and phosphines (Fig. 6). As expected, the stability of in situ generated Pd^I complexes supported by ^tBuN₄ was poor, as the hard amine ligands were a mismatch with the softer Pd^I metal ion. The transient EPR spectra showed an axial signal commonly associated with d⁹ complexes but exhibited a distinct lack of nitrogen hyperfine coupling, indicating that the axial amines were likely non-coordinating. Significantly greater stability was achieved using thioether-based pyridinophanes (obtained by chemical reduction of complexes **11** and **12**), as the softer sulfur donors would be expected to improve Pd^I complex stability (**13–15**). Unfortunately, the complexes had limited thermal stability and decomposed even at low temperatures, meaning full characterization and isolation was not possible [66]. The transient axial/pseudoaxial EPR spectra that could be obtained were similar to that of the ^tBuN₄ complexes, indicating that the sulfur donors did not have a tangible effect on the electronic structure of the observed Pd^I compounds. A dinuclear Pd^I compound supported by N2S2 with bridging ^tBuNC isocyanide ligands was isolated in the same study, implying that Pd^I compounds could indeed be stabilized with the thiapyridinophane ligand scaffold. In a related study, it was also found that **11** with acetonitrile as a supporting ligand was a competent electrocatalyst for CO₂ reduction with weak proton sources [67]. The catalyst was found to degrade over time and a decomposition pathway involving a dinuclear Pd^I carbonyl intermediate was identified.

In 2022, the Mirica group explored the incorporation bulky phosphine ligands as ancillary ligands, as the steric bulk could potentially prevent dimerization of Pd^I species [68]. With that in mind, the [Pd^I(P^tBu₃)₂]⁺ complex, reported previously by Chaplin and Ozerov, was reacted with thiapyridinophane ligands and was found to undergo rapid exchange with N2S2 and NCHS2 (3,7-dithia-1(2,6)-pyridina-5(1,3)-benzenacyclooctaphane) [69] to yield complexes **16** and **17** in ~70 % yields (Fig. 7). In the alternate synthetic procedure, the Pd^{II} analogs were synthesized by reacting the ligands with [Pd^{II}(MeCN)₄]²⁺, followed by ligation with P^tBu₃ to generate **18** and **19**. Well-defined reversible Pd^{II}/Pd^I redox waves for these complexes meant that **16** and **17** could be synthesized by chemical reduction with cobaltocene (CoCp₂). Both complexes exhibited distorted see-saw geometry, with a

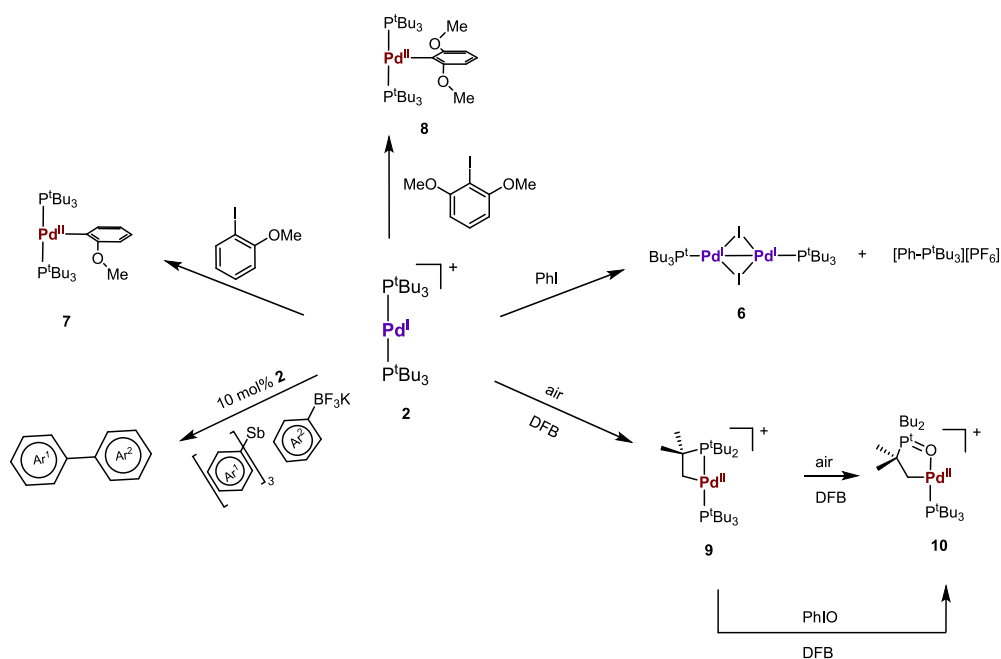


Fig. 5. Reactivity of the [Pd^I(P^tBu₃)₂]⁺ metalloradical. The counteranion for **9** and **10** is [PF₆][−].

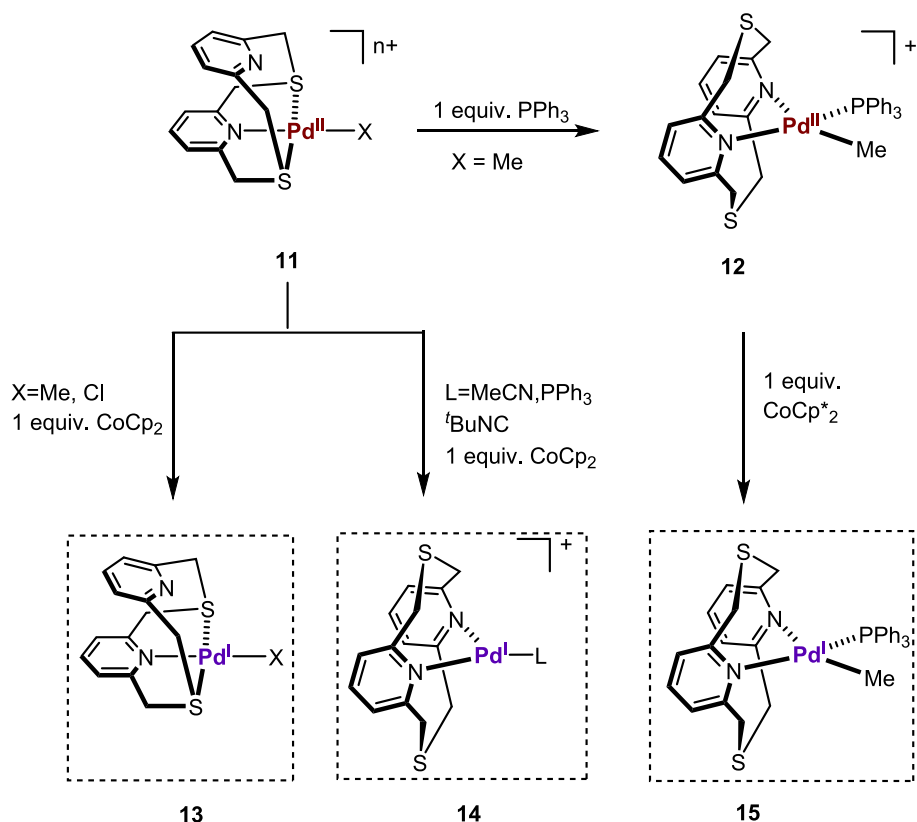


Fig. 6. Transient Pd^I species supported by thiapyridinophane ligands and with various ancillary ligands.

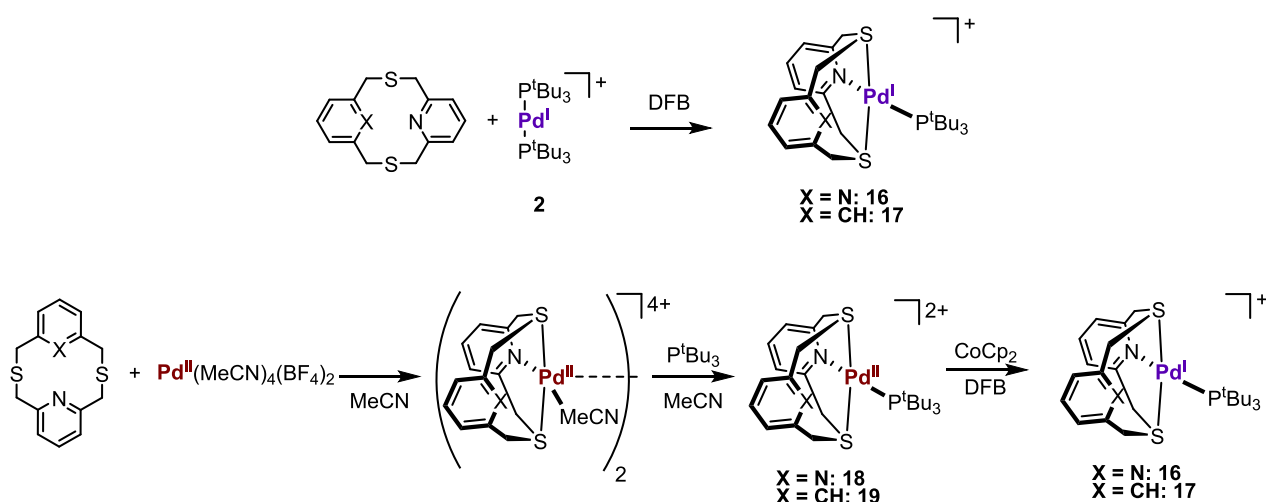


Fig. 7. Syntheses of (N₂S₂)Pd^I and (NCHS₂)Pd^I complexes.

four-coordinate Pd^I center. The N₂S₂ or NCHS₂ ligands bind via the two thioether S atoms and one N atom in a κ³ conformation, and the P^tBu₃ ligand completed the coordination environment.

Solution magnetic moments of 1.69 μ_B and 1.72 μ_B in DFB for **16** and **17** suggested the presence of one unpaired electron, confirming the presence of a d⁹ Pd^I species. EPR spectrum at 77 K, backed by DFT calculations shed further light on the electronics of the complex. Compound **16** had an axial signal ($g_x = g_y = 2.050$, $g_z = 2.219$) with characteristic superhyperfine coupling to the ³¹P atom, which was attributed to the presence of substantial electron density on the d_{x²-y²} orbital of the Pd center (~65 %) and with appreciable contributions from the remaining atoms. Similar electron densities were observed for **17**, but

loss of symmetry due to the presence of a phenyl group instead of a pyridyl group gave a rhombic EPR signal with $g_x = 2.030$, $g_y = 2.070$, $g_z = 2.237$. Both complexes were stable at low temperatures as evident from appreciable EPR signal intensities of the complexes at -80 °C for ~10 days.

Remarkably, **17** showed excellent catalytic competency in cross-coupling reactions between PhBr/PhI and cyclohexylMgCl to undergo Csp³-Csp² coupling, the first example of Csp³-Csp² Kumada coupling catalyzed by mononuclear Pd^I species (Fig. 8), supporting the direct role of Pd^I intermediates as proposed by Knochel et al. in 2009 [39]. Excellent yields were obtained with electron-rich and neutral bromides and cyclohexylmagnesium chloride, and similar yields were obtained with **2**

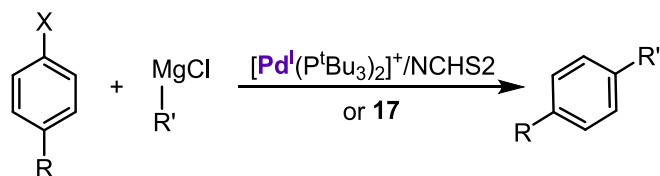


Fig. 8. Csp^3-Csp^2 Kumada cross-coupling catalyzed by mononuclear Pd^I species.

and NCHS2. In contrast, **16** did not show any such reactivity, probably due to the absence of an additional open coordination site.

2.3. Palladium(I) compounds stabilized by bidentate phosphine ligands

In 2021, Lancaster and Deng reported the first heteroleptic mononuclear Pd^I complex **21** without using P^tBu_3 as the supporting ligand system: $[(BINAP)Pd^I-(NHAr^{Trip})]$ (BINAP = 2,2'-bis(diphenylphosphino)-1,1'-binaphthalene, Ar^{Trip} = 2,6-bis(2',4',6'-triisopropylphenyl)phenyl). This system employs a wide bite angle bidentate phosphine BINAP ligand with a bulky anilide as the supporting group to provide kinetic inertness to the Pd^I center (Fig. 9) [70]. Such phosphines have been widely used for photoexcited Pd catalysis, [71,72] and this was the first Pd^I complex with π donating ligand, widely accepted as intermediates in such Pd-mediated photocatalytic processes [73]. Toluene solutions of $(BINAP)PdCl_2$ (**20**) and $LiNHAr^{Trip}$ were mixed at $-78^\circ C$, resulting in a blue-colored intermediate. Recrystallization at room temperature led to the isolation of green crystalline solids of **21**, and the compound was thoroughly characterized by elemental analysis, cold electrospray mass spectroscopy, and IR ($\nu_{N-H} = 3295\text{ cm}^{-1}$). Single crystal X-ray studies revealed a pseudo-trigonal planar Pd^I center with unequal P-Pd-N angles. Along with **21**, three amine byproducts were also observed, probably formed via the decomposition of the aminyl radical $[NHAr^{Trip}]^\bullet$. The Pd^I complex was proposed to be formed via the homolytic cleavage of the Pd—N bond of a Pd^{II} bisamido intermediate generated by the reaction of **20** with $LiNHAr^{Trip}$.

Counterintuitive to the fact that the trans influence of the amino ligand would elongate the Pd—P bond, the trans Pd—P bond was shorter than the cis Pd—P bond. This was attributed to the combined effect of $M \rightarrow PR_3$ π -backbonding and dispersion forces between the phenyl groups on the P atom of the BINAP ligand framework and those on 2,4,6-triisopropylphenyl group of the amido ligand. These dispersion forces ($\Delta E_{disp} = -31.3\text{ kcal/mol}$) and low Pd—N bond dissociation energy ($D_e = 50.9\text{ kcal/mol}$) help stabilize the Pd^I amido species at ambient conditions. Solution room temperature EPR spectra showed a four-line pattern centered at $g_{iso} = 2.052$. The g-anisotropy (consistent with DFT studies) was resolved by X-, Q-, and W-band EPR spectra, but was unusually different from previously reported Pd^I complexes ($g_1 = 2.0085$, $g_2 = 2.0350$, and $g_3 = 2.1115$). A magnetic moment of $2.1\ \mu_B$ confirmed the presence of an $S = 1/2$ species. Pd K- and L-edge X-ray absorption spectroscopy (XAS) data for **21** also confirmed the same. DFT studies indicated that **21** had a two-center, three-electron Pd—N π bond, and the singly occupied molecular orbital (SOMO) is highly delocalized, with

only 40 % Pd 4d orbital contribution. TD-DFT calculations revealed the origin of an intense feature at 808 nm in the UV–vis absorption spectrum, which was assigned to a $\pi \rightarrow \pi^*$ transition with ligand-to-metal charge transfer (LMCT) character.

Complex **21** was subjected to heat, irradiation, and ligand exchange with ancillary ligands, and underwent Pd—N bond homolysis to furnish anilines and Pd^0 species, which implies the formation of $[NHAr^{Trip}]^\bullet$ radical. When treated with phenols and amines, the free aniline was found to form in high yields along with Pd^0 complexes. These transformations were proposed to be initiated via proton transfer from the basic amido ligand of **21**, and a linear Hammett plot with a positive reaction constant was obtained for reactions of **21** with para-substituted anilines (Fig. 10). Moreover, no reactions were observed for compounds with weak C—H bonds like xanthene and cyclohexa-1,4-diene, ruling the possibility of a hydrogen atom abstraction mechanism.

Staying with the theme of using bidentate phosphines to stabilize Pd^I species, in 2024 the Gade group reported the first isolable Pd^I -carbonyl complex **26** (Fig. 11) [74]. Dinuclear Pd^I carbonyls have also been reported, in equilibrium with the monomeric form [75]. The carbazole-based (^{tBu}PNP) pincer-stabilized Pd^{II} -Cl complex **22** was first synthesized, followed by reduction with KC_8 to generate a naked Pd^I compound **24**. Single-crystal X-ray analysis revealed a T-shaped structure and a magnetic moment of $1.83\mu_B$ confirms the $S = 1/2$ ground state. EPR studies exhibited an isotropic signal centered at $g_{iso} = 2.105$, along with hyperfine coupling to the two ^{31}P and ^{14}N atoms. This agreed well with Mulliken population analysis, which unveiled $\sim 64\%$ electron density on the Pd center. To relate the Pd^I metalloradical to the potential diamagnetic Pd^{II} -hydrido complex, the neopentyl alkylated analog **23** was synthesized and hydrogenated to generate **25**. However, the former complex was thermally unstable and underwent homolytic Pd—C cleavage to generate **24**. Upon reaction of this naked Pd^I complex with carbon monoxide, the Pd^I -CO complex **26** was generated, as confirmed by the detection of a new EPR signal with reduced hyperfine coupling to Pd. These observations were attributed to the delocalization of the unpaired electron density from the metal center, leading to the population of the antibonding π^* orbital of CO. The reversibility of CO coordination was proved by the release of CO and immediate regeneration of **24** when the Pd^I -CO complex was depressurized in an inert environment. Single crystals of the Pd^I -CO compound featured a distorted square planar metal center with a bent CO attached to it. To explore the radical nature of **26**, its reaction with di(*tert*-butyl)disulfide was investigated. Typically, metalloradicals cleave disulfides to generate thiolate complexes, [76,77] and **24** in presence of CO led to the formation of **27**, which was structurally characterized by X-ray and IR ($\nu_{CO} = 1648\text{ cm}^{-1}$). DFT calculations were used to model the proposed mechanism, which revealed the reaction proceeds via C—S bond formation by the radicalized carbon of **26**.

2.4. Palladium(I) compounds stabilized by N-heterocyclic carbene ligands

Following the reasoning that sterically hindered, strong σ -donors like phosphines and N-heterocyclic carbenes (NHCs) could provide kinetic inertness to a mononuclear Pd^I center, de Jesus and coworkers used 1,3-

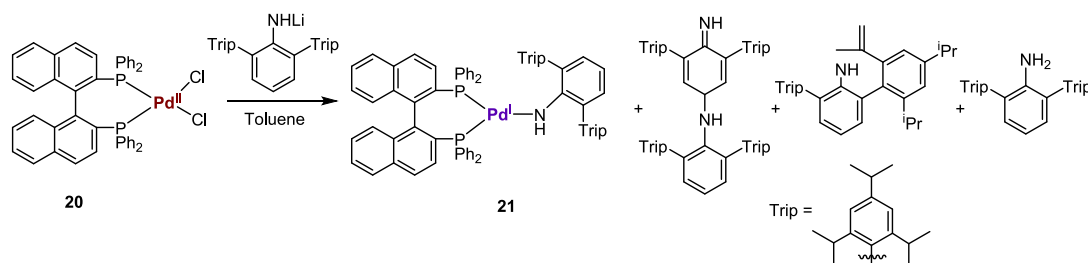


Fig. 9. Synthesis of BINAP-supported Pd^I -amido complex.

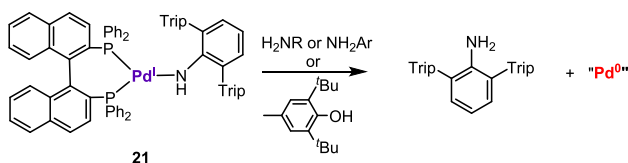
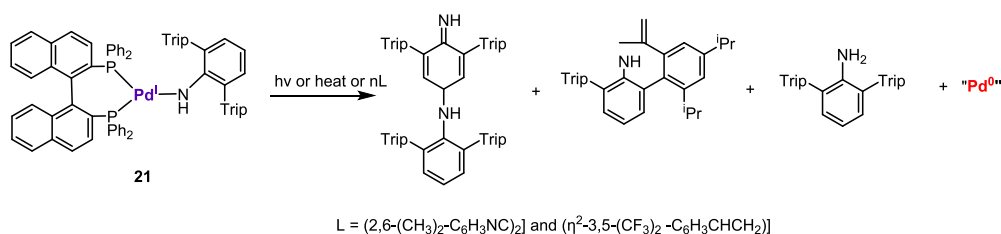


Fig. 10. Reactivity of Pd^I-amido complexes. “Pd⁰” for the first reaction refers to complexes [(BINAP)Pd(2,6-(CH₃)₂-C₆H₃NC)₂] and [(BINAP)Pd(η²-3,5-(CF₃)₂-C₆H₃CHCH₂)] formed by the reaction with the respective ligands “nL”. “Pd⁰” for the second reaction refers to complex (2,6-di-tert-butyl-4-methylenecyclohexa-2,5-dienone)Pd upon reaction with the ^tBu-substituted phenol.

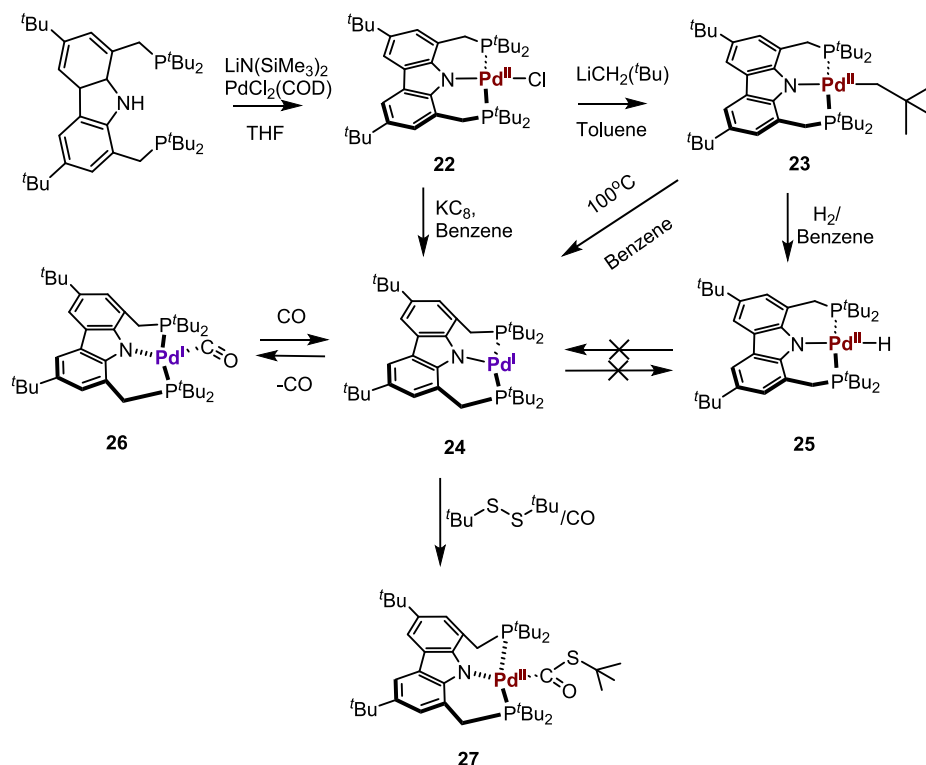


Fig. 11. Carbazole pincer-stabilized T-shaped Pd^I metalloradicals and their reactivity.

bis(2,6-diisopropylphenyl)imidazol-2-ylidene (IPr) to isolate and characterize a bench-stable Pd^I bis-carbene complex **29** (Fig. 12) [78]. Intending to design stable Pd^I complexes as reducing agents for small molecules such as O₂, they argued that the superior donation ability of NHCs as compared to phosphines could facilitate Pd^I to Pd^{II} oxidation [79,80]. In addition, the stability of metal-NHC bonds and wide availability of [Pd⁰(NHC)₂] precursors are some of the other advantages carbene have over phosphines [81]. Previous reports had showcased that O₂ could be reduced by [Pd⁰(NHC)₂] to generate the corresponding [Pd^{II}](η¹-O₂)₂ superoxides and [Pd^{II}](η²-O₂) peroxides [82,83].

Complex **28** showed reversible one-electron oxidation at -1.02 V in DFB (which is ~0.55 V less than **1**), reaffirming the fact that higher donicity of carbene facilitates Pd⁰ oxidation. The reaction of **28** with [Fc][PF₆] led to the formation of **29**, confirmed by an intense peak in the ESI-MS and a magnetic moment of 1.68μ_B. Crystallographic analysis

showed that **28** and **29** had similar structural parameters, [84,85] except for a marked increase in the M-C_{Carbene} distance as one moved from the neutral to the cationic species. The EPR spectrum revealed an axial signal with sextuplets arising from ¹⁰⁵Pd hyperfine coupling. A large coupling constant and high g anisotropy, backed by DFT calculations, indicated a metal-centered radical. All these observations are similar to the those reported by Chaplin and Ozerov in 2016, staying in line with features of M^I two-coordinate d⁹ complexes of group 10 metals. Although **29** was paramagnetic, the ¹H NMR spectrum was not very broad and allowed the assignment of resonance peaks. Variable temperature NMR experiments were performed, which agreed well with Curie's Law [86].

At low temperatures, the EPR spectra gave a different signal when a coordinating solvent like MeCN was used, pointing to partial formation of adduct **30**. Formation of an adduct at low temperature indicates the

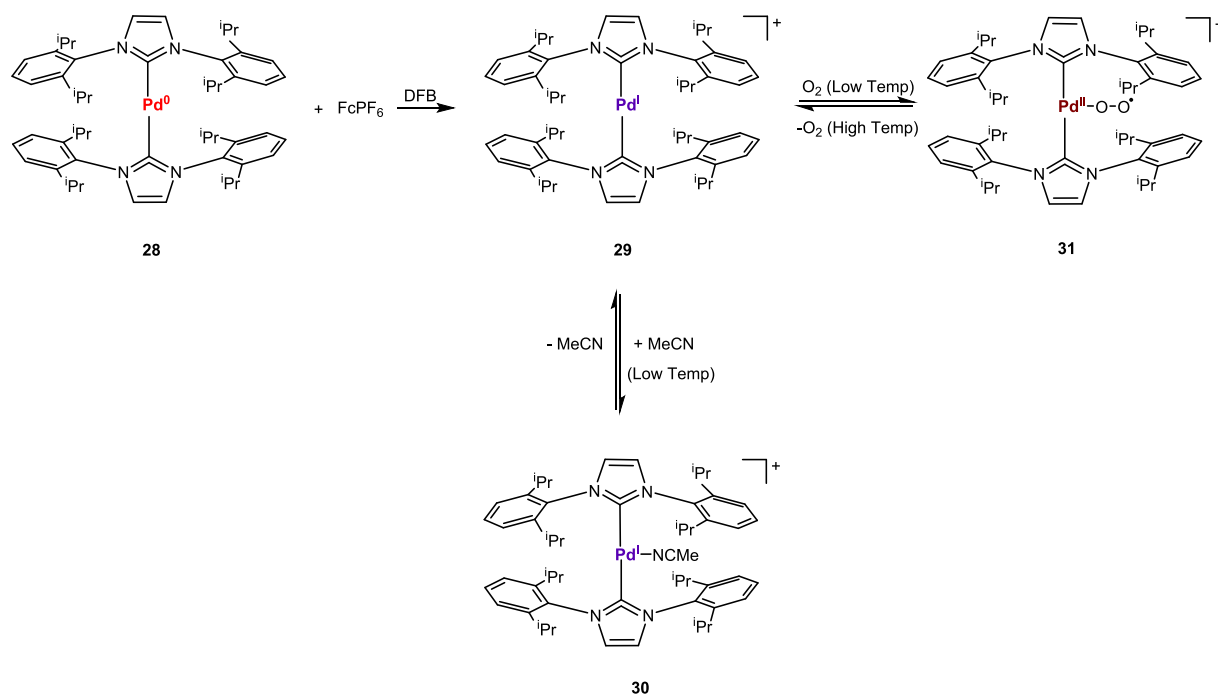


Fig. 12. Pd^I compounds stabilized by the N-heterocyclic carbene ligand IPr.

Pd atom's lower acidity and higher electronic richness in the carbene complex, as opposed to the synthesis of the acetonitrile adduct at ambient temperature with $[\text{Pd}^{\text{I}}(\text{P}^t\text{Bu}_3)_2]^+$. Although **29** was stable as a solid or in solution at ambient conditions, when pressurized under O₂ at lower temperatures generated a new paramagnetic species **31** as confirmed by a different EPR signal at 170 K that lacked hyperfine coupling to Pd. DFT calculations validated this observation, which revealed substantial spin density on the oxygen atoms. Complex **29** could be recovered quantitatively by heating **31** or removing O₂ under vacuum, implying that the binding was reversible.

A recent report from the Deng group reported compound **33**, the first Pd^I-aryl complex supported by a carbene framework (Fig. 13) [87]. The CF₃-substituted analog **33b** could activate carbon-halogen bonds of organic iodides and benzyl halide, enabling C_{aryyl}-C_{benzyl} cross-coupling.

The Pd^{II} precursor **32** was reacted with the corresponding aryl lithium salts, Ar^{Trip}Li(OEt₂) and p-CF₃-Ar^{Trip}Li(OEt₂) to obtain **33a** and **33b** in moderate yields (up to 59 %). Although air-sensitive, these complexes remained stable under nitrogen atmosphere and room temperature in solid form and in solution. ¹⁹F NMR analysis of a C₆D₆ solution of **33b** revealed that 90 % remained intact, while the rest decomposed to the corresponding arene and alkane chain dehydrogenation product. Both EPR spectra showed anisotropic signals and a sextet arising due to hyperfine Pd coupling, similar to previously reported Pd^I complexes. Computational calculations agreed well with this data, suggesting a massive 85 % unpaired electron density on the metal center. Single crystal X-ray analysis of the complexes featured a linear C-Pd-C core with a longer Pd-C_{carbene} bond than those in **29**, due to the aryl ligand's trans influence. Moreover, the bulky nature of the aryl ligand leads to

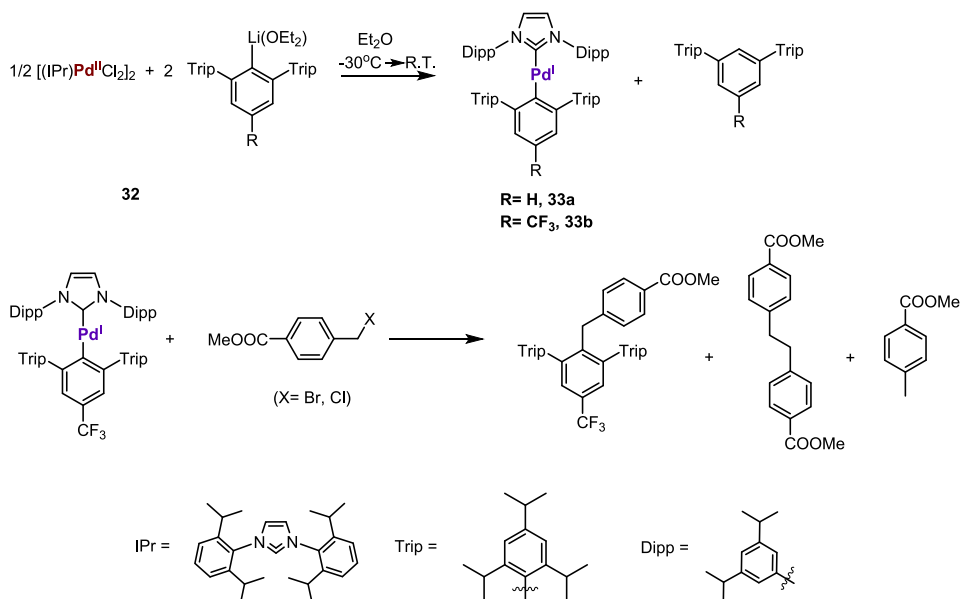


Fig. 13. Mononuclear Pd^I aryl complexes and their stoichiometric reactivity with organic halides.

steric repulsion with IPr, leading to non-planarity between the imidazole planes of IPr and the central arene. (dihedral angle of $\sim 41^\circ$) The aryl group at the Pd^I center underwent reactions with methyl 4-(bromomethyl)benzoate at room temperature to produce the cross-coupled product (75 % yield) along with the dehalogenation product and the benzyl radical coupled product. Cross-coupling reactions could also be performed with methyl 4-iodo-butanate, albeit the cross-coupled product was obtained in lower yields. It was proposed that the reaction path proceeds through single electron redox reactions between **33** and the organic halides, resulting in the formation of a Pd^{II} species and the organic radical. The long-lived alkyl and benzylic radicals could recombine with the Pd^{II} center to generate a Pd^{III} species, which could undergo reductive elimination to generate the cross-coupled product. Kinetic studies, radical trapping experiments, and DFT calculations revealed the reaction mechanism. Consumption of **33b** could be accelerated by the incorporation of electron-donating and electron-withdrawing groups on the para position of the benzyl bromide. When a mixture of **33b** and methyl 4-(bromomethyl)benzoate was reacted with classical radical traps like TEMPO (2,2,6,6-tetramethylpiperidine-1-oxyl) and DMPO (5,5-dimethyl-1-pyrrolineN-oxide), the corresponding benzylic-TEMPO and DMPO radical adducts were detected using NMR and EPR respectively. DFT analyses revealed that the cross-coupling reaction was initiated by an inner sphere electron transfer process and the Pd^{III} intermediate underwent reductive elimination to yield the cross-coupled product.

3. Mononuclear palladium(III) compounds

3.1. Homoleptic Pd(III) complexes stabilized by facially-chelating tridentate ligands

The first examples of structurally and spectroscopically Pd^{III} coordination complexes are the Werner-type compounds supported by tridentate facially chelating macrocyclic ligands. In fact, the first reported mononuclear Pd^{III} compound was a homoleptic 2:1 coordination complex of the tridentate macrocyclic ligand 1,4,7-trithiacyclononane (ttcn), **34**, by Schröder and coworkers in 1987 (Fig. 14) [88]. The same group also reported the Pd^{III} complex **35** of an expanded thioether-based macrocycle [18]aneS₆ in 2012 [89]. The electrochemistry of the Pd^{II} precursor for **34** revealed a reversible Pd^{II/III} redox wave at +0.57 V vs Fc^{+/0}, while no discernible redox event was seen for the Pd^{II} precursor for **35**. The corresponding Pd^{III} complexes were synthesized as their hexafluorophosphate or perchlorate salts by oxidizing the Pd^{II} precursors either by electrochemical oxidation in 0.2 M ⁿBu₄PF₆/MeCN or using a chemical oxidant like 70 % HClO₄. X-ray diffraction analysis revealed that **34** and **35** adopt a Jahn-Teller distorted octahedral geometry, in accordance with the d⁷ electronic configuration, with relatively shorter axial Pd–S distances (2.5356 Å) and longer equatorial Pd–S bond lengths by approximately 0.05–0.06 Å as compared to their Pd^{II} counterparts. Extensive EPR studies for the Pd^{III} complexes at variable frequencies and temperatures show similar g-values for g_{xx} (2.048) and g_{yy} (2.046 for **34** and 2.036 for **35**, respectively), corresponding to the contributions from the equatorial plane. Lower g_{zz} values, 2.004 for **34** and 1.998 for **35**, were found for the axial contributions. Finally,

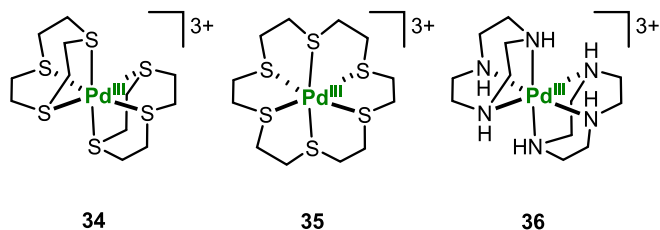


Fig. 14. Molecular structures of the Pd^{III} salts supported by macrocyclic ligands.

detailed DFT calculations were undertaken to elucidate the electronic structure of these macrocyclic thioether-ligated Pd^{III} compounds. Significant delocalization of the spin density away from the Pd^{III} center was seen, with the SOMO showing 26–27 % Pd 4d_{z²} character. The thioether sulfur atoms were found to contribute nearly 62 % to the SOMO, implying that the thioether sulfur atoms show redox non-innocence in these compounds.

The same group also reported a homoleptic 2:1 Pd^{III} compound **36** with the analogous nitrogen containing macrocycle 1,4,7-triazacyclononane (tacn) [90]. The observed Pd^{II/III} oxidation of the parent [Pd^{II}(tacn)₂]²⁺ compound was reported to be 0.07 V vs Fc^{+/0}, indicating that the harder secondary amines thermodynamically favor the Pd^{III} state compared to the softer thioether groups. Controlled potential electrolysis experiments revealed the formation of a species exhibiting an EPR signal with g = [2.123, 2.007] and superhyperfine coupling to two nitrogen atoms (A = 27 G). The PF₆⁻ salt of **36** was analyzed by SC-XRD and displayed similar tetragonal distortion to the ttcn analog **35**, with the axial Pd–N distances elongated by 0.07 Å compared to the equatorial Pd–N distances of ~ 2.115 Å. Interestingly, the authors noted that the tacn analog was more stable in solution than the ttcn analog, yet again accentuating the hard/soft mismatch. More recently, the methylated version of tacn, Me₃tacn, has been used to stabilize halide-bridged dinuclear Pd^{III} complexes, although such complexes are beyond the scope of this review [91].

3.2. Palladium(III) compounds stabilized by pyridinophane ligands

After the reports by Schröder and coworkers presented above, the organometallic chemistry of Pd^{III} compounds remained dormant for two decades before the Mirica group reported the first examples of mononuclear organometallic Pd^{III} complexes supported by multidentate macrocyclic ligands that stabilized multiple oxidation states by adapting to the geometric preferences of the Pd^{III} center (Fig. 15). This was a significant advance as the direct reductive elimination of organometallic ligands bound to a high-valent Pd center, which had been proposed by Mayer and Sanford (vide infra), could now be studied from well-defined, structurally characterized compounds.

The ligand of choice for these studies was the tetradentate macrocycle *N,N'*-dialkyl-2,11-diaza[3.3](2,6)pyridinophane (abbreviated as ^RN₄ throughout this review, where R = alkyl). The first transition metal complex supported by this ligand scaffold was a (^RN₄)Cu^ICl₂ complex (R = ^tBu, Me, or Bz) reported by the Che group in 1994 [63]. Interestingly these compounds exhibited a distorted octahedral geometry, with the axial tertiary amines binding to the Cu center significantly deviating from the optimal 180° bond angle. The geometrically enforced distorted octahedral environment resembles the Jahn-Teller distortion that would

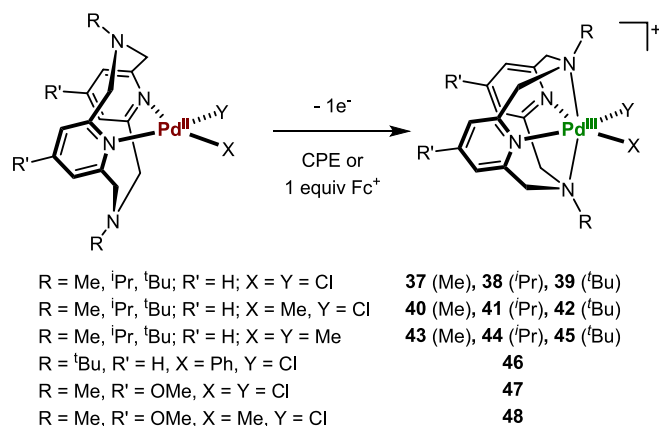


Fig. 15. Synthesis of mononuclear Pd^{III} compounds that are supported by ^RN₄ ligands with various ancillary ligands by the oxidation of the corresponding Pd^{II} precursors. Complexes **37–48** represent Pd^{III} complexes.

be preferred for a d^7 metal ion, and this property of the pyridinophane macrocycles plays a key role in their high-valent palladium coordination chemistry.

The first reports from Mirica and coworkers were a set of mononuclear Pd^{II} and Pd^{III} complexes supported by the R^N4 ligand framework (Fig. 15) [92–94]. It was shown that the R^N4 ligands facilitated in lowering the $Pd^{II/III}$ redox potential such that mild oxidizing conditions could be employed. Accordingly, both electrochemical and chemical oxidation were employed to synthesize the corresponding Pd^{III} complexes 37–48. The key to the stabilization of both Pd^{II} and Pd^{III} states was the conformational flexibility of the R^N4 ligands. The neutral 16-electron Pd^{II} compounds favor a square-planar geometry with the R^N4 ligand adopting a bidentate binding mode, and the solid-state structures of the Pd^{II} compounds indeed reveal that the tertiary amines had no interaction with the Pd center. However, upon one-electron oxidation, the Pd^{III} center exhibits appreciable axial interactions with the amine N's. Solid-state structural analysis revealed the Jahn-Teller-like distorted octahedral geometries of the d^7 Pd^{III} center. Significantly longer axial Pd– N_{amine} bond lengths of 2.41–2.48 Å were found, compared with the shorter Pd– $N_{pyridyl}$ bonds which forms the equatorial plane with the ancillary ligands X and Y as shown in Fig. 15 [95]. The nature of the alkyl groups of the axial tertiary amines critically influences the structure and reactivity of these Pd^{III} compounds, as discussed below.

3.2.1. Spectroscopic properties of Pd^{III} complexes supported by pyridinophane ligands

The electronic properties of the $(R^N4)Pd^{III}$ complexes were first probed by EPR, and they were found to display either axial or rhombic spectra, with average g values ranging from 2.11 to 2.14. The simulation parameters were consistent with a d_{z^2} ground state, along with strong superhyperfine coupling to two $S = 1$ ^{14}N nuclei, supporting the strong interaction between Pd^{III} and the axial nitrogens [92,94]. The ligand field environments correspond directly to the symmetry of the individual axes, showing rhombic signals in 40–42 and 46, and more symmetric axial signals for 43–45. DFT calculations corroborated that the unpaired electron is localized on the Pd-based d_{z^2} orbital, proving the metal-radical nature of these compounds. Time-dependent DFT studies were performed to understand the nature of the transitions that give rise to the three characteristic absorption bands at 723–741, 554–594, and 353–386 nm. They were assigned as LMCT transitions, a combination of LMCT and d-d transitions, and LMCT transitions, respectively [92].

3.2.2. Stereoelectronic effects of ligand modification on the properties of Pd^{III} compounds

The alkyl N-substituents of the R^N4 ligands were shown to be critical in tuning the redox properties of the Pd^{II} compounds, particularly with respect to the $Pd^{II/III}$ oxidation. The Me^N4 , iPr^N4 , and tBu^N4 ligands were used to study the structure and reactivity of the corresponding $Pd^{III}MeCl$ and $Pd^{III}Me_2$ complexes [96]. Interestingly, the oxidation potentials of all complexes increased with an increase in steric bulk. For example, the oxidation potential of 40, 41, and 42 increases from -0.480 V to $+0.010$ V to $+0.134$ V, respectively (Fig. 16). Additionally, crystallographic analysis of these complexes showed a distinct lengthening of the Pd– N_{axial} bond distances in steps of approximately 0.05 Å with increasing steric bulk. Furthermore, the observed trends are also consistent for the UV–Vis and EPR parameters. Increasing steric bulk results in a red-shift of the d-d absorption feature in the UV–Vis spectra, going from 606 nm to 658 nm to 723 nm for the $[(Me^N4)Pd^{III}MeCl]^+$, $[(iPr^N4)Pd^{III}MeCl]^+$, and $[(tBu^N4)Pd^{III}MeCl]^+$ complexes, respectively. This trend continues for the analogous $Pd^{III}Me_2$ compounds, going from 620 nm to 666 nm, to 741 nm, respectively. Two interesting structural conclusions could be drawn from the EPR parameters, the rhombicity of the g tensor values and the degree of hyperfine coupling from the axial amine N's. In general, rhombicity was seen to increase with increased steric bulk (for example g_{avg} increases with steric bulk, but the value of g_z remains relatively constant). Additionally, the degree of superhyperfine coupling decreases with steric bulk, going from A_{2N} values of 23.0 G to 21.3 G to 19.5 G for the $[(Me^N4)Pd^{III}MeCl]^+$, $[(iPr^N4)Pd^{III}MeCl]^+$, and $[(tBu^N4)Pd^{III}MeCl]^+$ complexes, respectively. The combination of all these factors indicates that increasing steric bulk results in a distinct weakening of the Pd– N_{axial} interaction, destabilizing the Pd^{III} state. In general, smaller alkyl substituents enforce a more symmetric octahedral geometry compared to the bulkier ones, which leads to the observed solid-state and solution features of the Pd^{III} compounds.

To explore the combined stereoelectronic effect of ligand modifications on the spectroscopic properties of the Pd center, the electron-rich p -OMe Me^N4 ligand and its Pd complexes were synthesized [94]. While electronic modification of the ligands typically has drastic consequences on the properties of the corresponding metal complexes, the presence of the electron donating -methoxy groups had little effect on the structural and electronic properties of the $Pd^{III}Cl_2$ and $Pd^{III}MeCl$ (47 and 48) complexes, especially compared to the drastic impacts of steric

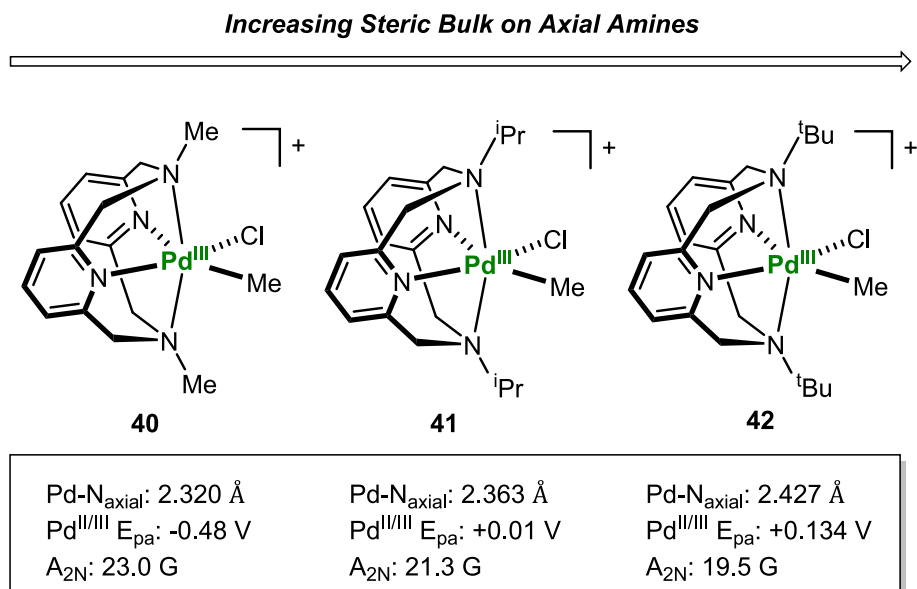


Fig. 16. Influence of the steric bulk of axial amine N-substituents on the spectroscopic and structural properties of the $[(R^N4)Pd^{III}MeCl]^+$ complexes (R = Me, iPr , or tBu).

modification (Fig. 17). The Pd^{II/III} redox potentials for (*p*-OMe^{Me}N4)Pd^{II} complexes showed only a slight negative shift in potential (~20 mV) for the more electron-rich Pd^{II} compound. Furthermore, the Pd^{III} complexes only showed a modest red-shift in the absorption features of the *p*-OMe versus the *p*-H analogue: 583 vs 578 nm for the [(^RN4)Pd^{III}Cl₂]⁺ complexes, and 615 vs 606 nm for the [(^RN4)Pd^{III}MeCl]⁺ complexes, respectively. EPR spectra for these complexes also showed nearly identical *g* tensor values and hyperfine coupling constants. Structurally, all complexes showed distorted octahedral environments around the Pd^{III} centers, with no changes (within error) in the metrical parameters regardless of using the *p*-OMe versus the *p*-H^{Me}N4 ligand analog, further highlighting the lack of ligand electronic effects on the corresponding Pd complexes. Electronic density calculations of the HOMO and LUMO orbitals show very little donation from the pyridines into the Pd^{III} centers, which may explain the lack of observed spectroscopic differences. Finally, recent XAS studies support the electronic trends observed via the various spectroscopic studies described above [97].

3.2.3. Electrochemical evaluation of the conformational flexibility of ^tBuN4 in stabilizing Pd^{III} complexes

One interesting question to address was the solution speciation of the various conformers of the (^RN4)Pd^{II} complexes in solution, given the flexibility of the ^RN4 ligands and the profound effect the axial amine binding has on the spectroscopic properties and reactivity of these Pd complexes. Extensive electrochemical studies were performed by the Mirica group to reveal the intricacies of the solution structure of the Pd complexes supported by the ^tBuN4 ligand. The cyclic voltammetry studies conducted at various scan rates and variable temperatures revealed that the conformational flexibility of the axial amines of ^tBuN4 ligand allows it to adopt different binding modes, namely bidentate (κ^2), tridentate (κ^3), or tetradentate (κ^4) ligations. The oxidation of the Pd^{II} precursors becomes more thermodynamically favorable as the pre-positioning of the axial tertiary amines allows the stabilization of Pd^{III} centers (Fig. 18) [98]. It was also found that lowering the temperature slows down the conformational changes from temperature-dependent cyclic voltammetry. At lower temperatures, the dominant electrochemical response is the Pd^{II/III} oxidation arising from the κ^3 conformer, indicating even a tridentate coordination is sufficient to stabilize Pd^{III}. On the other hand, raising the temperature facilitates the rapid conformational changes which lead to the observed electrochemical response from both κ^3 and κ^4 conformers. Overall, the studies led the authors to conclude that the contribution of each axial amine donor towards lowering the Pd^{II/III} oxidation potential was ~0.6 V (Fig. 18). Thus, the pre-positioning of the axial amines in a κ^4 ligation mode lowers the Pd^{II/III} potential by nearly 1.2 V. In the same report, a dicationic Pd^{III} complex [(^tBuN4)Pd^{III}Me(MeCN)]²⁺, **49**, was isolated by abstracting the chloride in **42** with a silver salt. **49** has shorter axial Pd–N_{amine} bonds compared to the analogous monocationic Pd^{III} complex **42**, attributed to a stronger electrostatic attraction between the Pd center and the lone pairs of the amine N donors (Fig. 19).

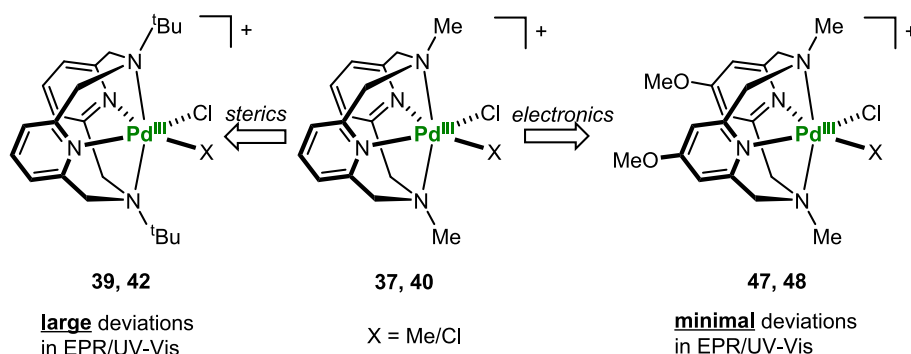


Fig. 17. Steric versus electronic effects of ^RN4 ligand modifications on the corresponding (^RN4)Pd^{III} compounds.

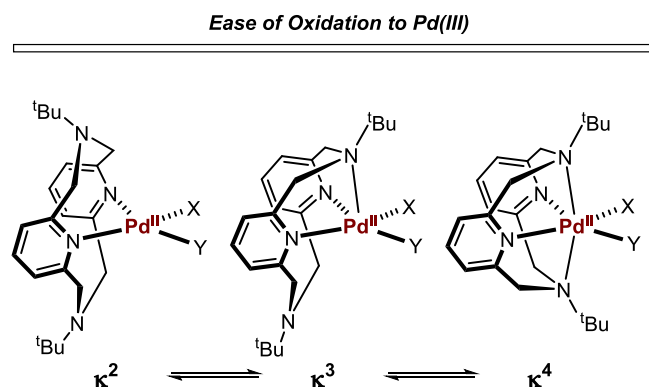


Fig. 18. The three conformations of (^RN4)Pd^{II} compounds shown to exist in solution and their relative ease of oxidation. X and Y are placeholders for ancillary ligands and hence the charge of the complexes is not shown.

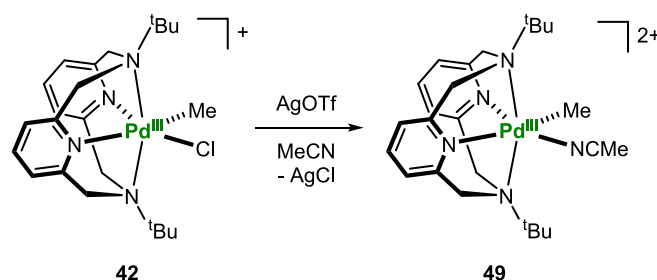


Fig. 19. Synthesis of a rare dicationic [(^tBuN4)Pd^{III}(Me)(MeCN)]²⁺ complex.

A fundamental insight that came from these studies was that the oxidation of the Pd^{II} compounds is not governed by the most predominant species in solution, the κ^2 conformer. Rather, the higher denticity conformations, which can be more easily oxidized dictates the redox chemistry of these compounds. The κ^3 or κ^4 conformers are formed via an EC (electrochemical step followed by chemical step) mechanism, which was fully supported by the simulations of the respective CVs.

3.2.4. Reactivity of pyridinophane-supported Pd^{III} complexes

The isolation of well-defined Pd^{III} organometallic compounds have allowed for the detailed analysis of their reactivity profiles. As discussed in the preceding sections, the spectroscopic effects of ligand modifications, either on the backbone or the axial amines laid down the foundation to understand the C–C bond formation reactivity of the Pd^{III} compounds supported by pyridinophane ligands. This section highlights the reactivity of the Pd^{III} organometallic compounds in the context of aerobic oxidation, allylic amination, and C–H activation. The report from Mayer, Sanford, and coworkers provided chemical and spectroscopic evidence for the intermediacy of Pd^{III} in the reductive elimination

of ethane from a bipyridine-ligated Pd^{II} dimethyl complex [38]. The isolation of complexes **42**, **45**, and **46** by the Mirica group enabled a direct study of the reductive elimination reactivity of alkyl and aryl groups bound to a Pd^{III} center (Fig. 20). It was shown that light-induced reductive elimination of ethane was feasible starting from both monomethyl and dimethyl Pd^{III} complexes **42** and **45**. Similar reductive elimination of biphenyl was also observed starting from the monophenyl complex **46**. Various methyl radical traps were used to prove the generation of methyl radicals. Additionally, **42** and **46** were shown to undergo crossover reactivity under irradiation, generating toluene. Critically, this provided the first evidence that ethane formation was feasible from the monomethyl Pd complex **42**, via methyl group transfer steps.

The next foray into the chemistry of (^tBuN4)Pd compounds was the reactivity of the Pd^{II}Me₂ complex in the presence of oxidants [93]. Due to the a low Pd^{II/III} oxidation potential of **45**-Pd^{II}, exposure to O₂ resulted in rapid formation of the oxidized [(^tBuN4)Pd^{III}Me₂]⁺ complex, likely supported by a hydroxide counteranion. Evidence for this was obtained from the identification of a Pd^{II}(Me)(OH) species as the final product. This reaction could be conveniently tracked by UV–Vis due to a strong absorption feature at 750 nm ($\epsilon = 639 \text{ M}^{-1} \text{ cm}^{-1}$). EPR measurements revealed superhyperfine coupling to the two axial N atoms in $g_z = 1.986$ direction, and to a lesser extent in the $g_x = 2.221$ and $g_y = 2.191$ directions. These values are consistent with the crystallographically observed distorted octahedral coordination environment with similar ligand fields in the x and y directions [99]. Interestingly, exposing **45**-Pd^{II} to oxygen eventually led to the formation of ethane in 52 % yield, demonstrating significant oxidative reactivity (Fig. 21). Radical trapping experiments show inhibition of ethane formation with TEMPO, and crossover experiments with the deuterium labeled Pd^{II}(CD₃)₂ derivative shows formation of a statistical amounts of the CH₃-CH₃, CH₃-CD₃, and CD₃-CD₃ isotopologs in the reaction. Altogether, this indicates that a disproportionation event occurs to generate a Pd^{IV}Me₃ complex along with a Pd^{II} species that is capable of methyl group transfer to generate ethane. Related to this O₂ activation reactivity, the Mirica group recently reported electrocatalytic oxygen reduction by the related complex **42** and showed that a key dinuclear Pd^{III}-peroxo intermediate is involved in the generation of water from molecular oxygen and proton sources (acetic acid or sulfuric acid) in water [100].

In order to further probe the aerobically-induced methyl group transfer process, a modified ligand framework bearing methyl N-

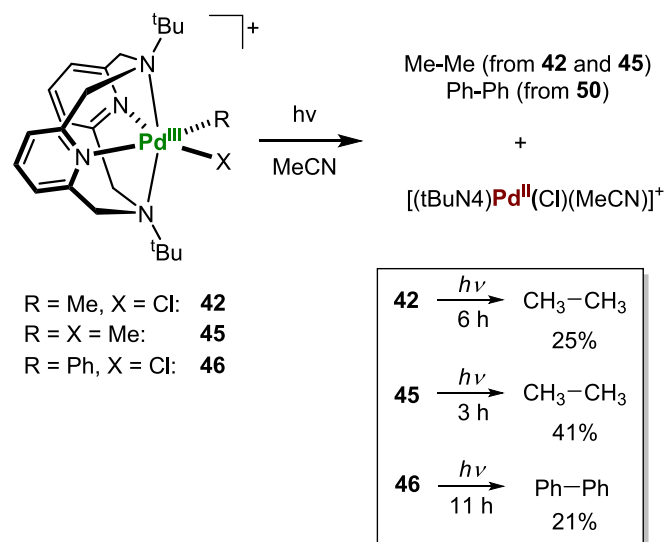


Fig. 20. Photoinduced ethane or biphenyl formation from organometallic (^tBuN4)Pd^{III} complexes.

substituents (^{Me}N4) was synthesized [101]. It was hypothesized that the smaller steric profile of the N-methyl groups would allow for greater stability of the corresponding octahedral Pd^{IV} species formed during the reaction. Interestingly, in the presence of O₂, **43**-Pd^{II} was found to generate a Pd^{IV} compound **47**, which was crystallographically characterized and shown to bear three methyl groups and a κ^3 -^{Me}N4 ligand binding mode (Fig. 22), and thus confirming an intermolecular methyl group transfer. Additionally, exposing the Pd^{II} precursor to methyl iodide generated the same Pd^{IV} complex and subsequently formed ethane in high yields. Additionally, NMR indicated that the methyl groups were identical in solution, suggesting a fluxional conformation of the three methyl groups. ESI-MS revealed the formation of Pd^{IV}-peroxide and Pd^{IV}-hydroxide species, suggesting an inner-sphere O₂ activation process that is feasible due to the flexible nature of the pyridinophane ligand scaffold.

While significant progress had been made in understanding the factors that stabilize high-valent Pd species supported by pyridinophane ligands, the reactivity left room for improvement. A significant advance in improving the C–C bond formation was achieved through the use of the pseudo-tridentate pyridinophane ligand N-methyl-N'-tosyl-2,11-diaza[3.3](2,6)pyridinophane (^{TsMe}N4) [102]. This unsymmetric pyridinophane contains a strongly-coordinating methyl group as well as a weakly coordinating N-tosyl group. It was hypothesized that a N-tosyl group would drive ligand dissociation by decreasing the affinity of the axial nitrogen towards the Pd center. Electrochemically, the same fluxional ligand behavior was observed for the (^{TsMe}N4)Pd^{II} complexes **48**, with an anodic shift in oxidation potentials consistent with the increase in steric bulk and low coordinating ability of the N-tosyl group. Attempts to oxidize the (^{TsMe}N4)Pd^{II}-dimethyl compound resulted in no detected Pd^{III} species, likely due to decreased stability, and a significant decomposition of [(^{TsMe}N4)Pd^{III}MeCl]⁺ and [(^{TsMe}N4)Pd^{III}Cl₂]⁺ species **49** was observed within 2 h, their limited stability thus diverging from those of the previous (^RN4)Pd^{III} complexes (Fig. 23). The EPR signals of [(^{TsMe}N4)Pd^{III}MeCl]⁺ and [(^{TsMe}N4)Pd^{III}Cl₂]⁺ showed a large decrease in the magnitude of nitrogen superhyperfine coupling to values of 10 G and 5 G for (^{TsMe}N4)Pd^{III}Cl₂ and [(^{TsMe}N4)Pd^{III}MeCl]⁺, respectively, vs. superhyperfine coupling constants of 35.5 G and 31.5 G for the (^{Me}N4)Pd^{III} analogs, and thus confirming the weakly coordinating nature of the N-tosyl group. The (^{TsMe}N4)Pd^{II}Me₂ complex lead to a high yield of ethane formation upon oxidation with air and faster reaction rates than the for other ^RN4 scaffolds. A significant improvement in the yield of ethane formation was observed when methyl iodide was used as an oxidant, which generated ethane in 89 % yield with stoichiometric methyl iodide, and quantitative ethane formation with excess methyl iodide [103]. ESI-MS experiments indicate the formation of the [(^{TsMe}N4)Pd^{IV}Me₃]⁺ intermediate, which had been proposed in previous studies (Fig. 23).

Pd-catalyzed allylic functionalization is a cornerstone reaction in modern organic synthesis, [104,105] and high-valent Pd-allyl species have been proposed in various bond formation reactions [106]. The Mirica group also reported a study demonstrating a Pd-mediated allylic amination reaction facilitated by high-valent Pd intermediates (Fig. 24) [107]. Pd^{II}-allyl complexes bearing N4-type ligand scaffolds can be prepared by direct ligand exchange of ^RN4 (R = ^tBu or Me) with well-known and commercially available [Pd^{II}(η^3 -allyl)(Cl)]₂ or [Pd^{II}(η^3 -cinnamyl)(Cl)]₂ precursors in the presence of AgPF₆ to generate monomeric [(^RN4)Pd^{II}(η^3 -allyl)]⁺ complexes. In these complexes, the ^RN4 ligand adopts a κ^3 binding mode, with both pyridine groups and one axial amine group binding to give distorted square pyramidal geometries, unexpected for organometallic Pd^{II} compounds. Oxidation of these species in the presence of thianthrenyl hexafluorophosphate (ThnPF₆) or acetylferrocenium hexafluorophosphate (^{Ac}FcPF₆) gave the proposed Pd^{III} analogs. The [(^tBuN4)Pd^{III}(η^3 -allyl)]²⁺ species displayed a rhombic EPR spectrum with superhyperfine coupling to two axial N donors ($A_{2N} = 22 \text{ G}$), and suggesting the ^RN4 ligand adopts a κ^4 binding mode in these Pd^{III} complexes **51** (Fig. 24). This species was found to be highly

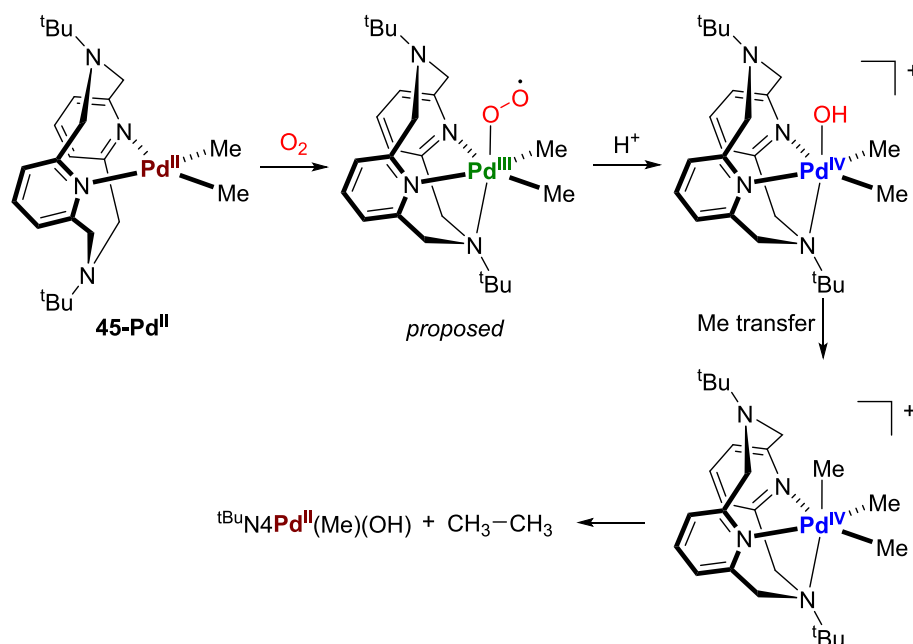


Fig. 21. Aerobic reactivity of the $(^{\text{tBu}}\text{N}_4)\text{Pd}^{\text{II}}\text{Me}_2$ complex.

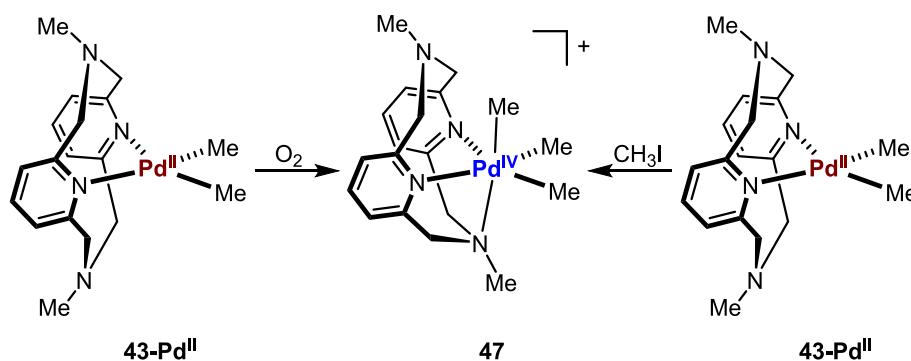


Fig. 22. Formation of a $(^{\text{Me}}\text{N}_4)\text{Pd}^{\text{IV}}$ compound as an intermediate for ethane formation from the $(^{\text{Me}}\text{N}_4)\text{Pd}^{\text{II}}\text{Me}_2$ complex.

unstable, with decay happening with one minute at room temperature. By comparison, no EPR spectrum was observed for $(^{\text{Me}}\text{N}_4)\text{Pd}^{\text{II}}(\eta^3\text{-allyl})^+$ oxidation at -35°C . However, on lowering the reaction temperature to -94°C resulted in the formation of an EPR spectrum which was proposed to be a mixture of the allyl ligand binding to the Pd^{III} center in η^3 and η^1 hapticities (50 and 51 in Fig. 24). Pd^{IV} -allyl complexes are known to prefer the η^1 binding mode, [108–110] and the observation of interconversion between the two at Pd^{III} was a proof of intermediacy. Furthermore, the isomerization appears to be dependent on the identity of the allyl fragment, as 2-methylallyl did not appear to isomerize to the η^1 geometry upon oxidation. As the complexes demonstrated a high degree of instability, their reactivity was probed in the presence of electrophilic oxidants. Exposing these allyl complexes to *N*-fluorobenzenesulfonimide (NFSI) resulted in the rapid C–N bond formation to generate allyl- $\text{N}(\text{SO}_2\text{Ph})_2$ species in moderate yields (Fig. 24), generating the $[(^{\text{R}}\text{N}_4)\text{Pd}^{\text{III}}(\text{MeCN})_2]^{3+}$ species in the process. It is proposed that the reaction proceeds through a Pd^{IV} intermediate after two-electron oxidation by NFSI, followed by reductive elimination to give Pd^{II} complexes that are subsequently reoxidized to Pd^{III} . Remarkably, this reactivity demonstrates for the first time that pyridinophane-supported Pd species are capable of mild and rapid C–N bond formation reactions.

One of the most important modern chemical transformations is C–H bond activation, however, a lack of bond polarizability and chemical

selectivity is an ongoing issue. While C–H bond activation at Pd^{II} or Pd^{IV} centers have been well-characterized, C–H activation at Pd^{III} is very rare. The organometallic cycloneophyl ligand framework has been used for many years as a model system for nickel organometallic reactivity due to its high stability, [111,112] and the preparation of the palladium analogue was first reported in 2001 by Cámpora and co-workers [113]. Using a combination of the $^{\text{Me}}\text{N}_4$ ligand and a Pd-cycloneophyl moiety, the Mirica group reported the first example of C–H activation at a Pd^{III} center, tracking the reaction by both UV–Vis and EPR spectroscopy [114]. Mechanistic investigation demonstrated that this process was mediated by a CMD-type mechanism with exogenous acetate, analogous to similar transformations at Pd^{II} and Pd^{IV} oxidation states, [115–117] showing the universal nature of this reaction pathway. Furthermore, the reaction appears to proceed through dissociation of one of the axial amine ligands for 52 to facilitate the CMD transition state, highlighting the necessity of the flexible nature of the pyridinophane scaffold (Fig. 25). An oxidative C–H bond activation was also reported where exposing the $(^{\text{Me}}\text{N}_4)\text{Pd}^{\text{II}}(\text{neophyl})\text{Cl}$ complex 52 to O_2 gas resulted in the direct generation of the $[(^{\text{Me}}\text{N}_4)\text{Pd}^{\text{III}}(\text{cycloneophyl})]^+$ complex 53, indicating the possibility of aerobic Pd-mediated C–H bond functionalization under mild conditions.

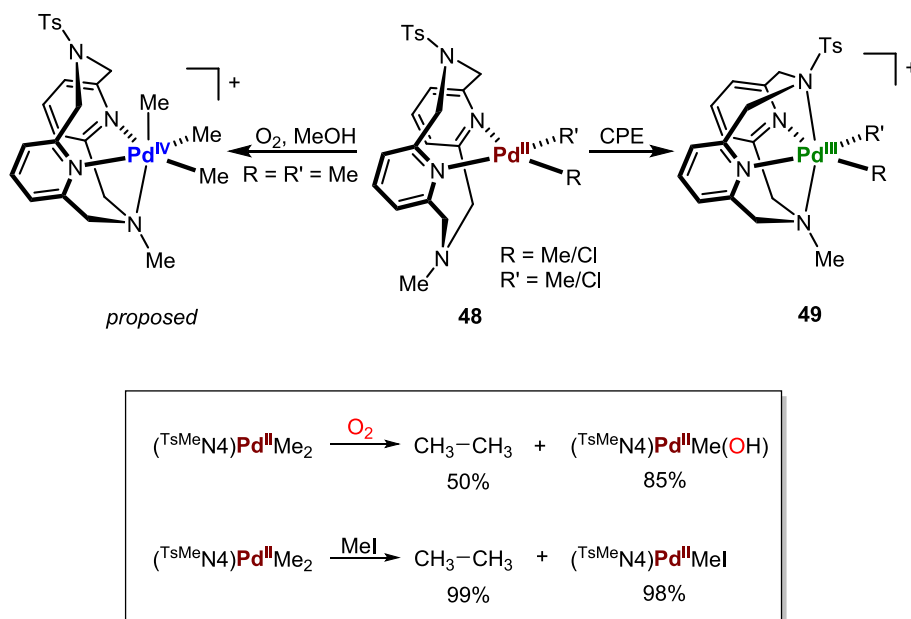


Fig. 23. Aerobic and oxidative reactivity of Pd complexes supported by a pyridinophane ligand bearing a hemilabile arm, TsMeN_4 .

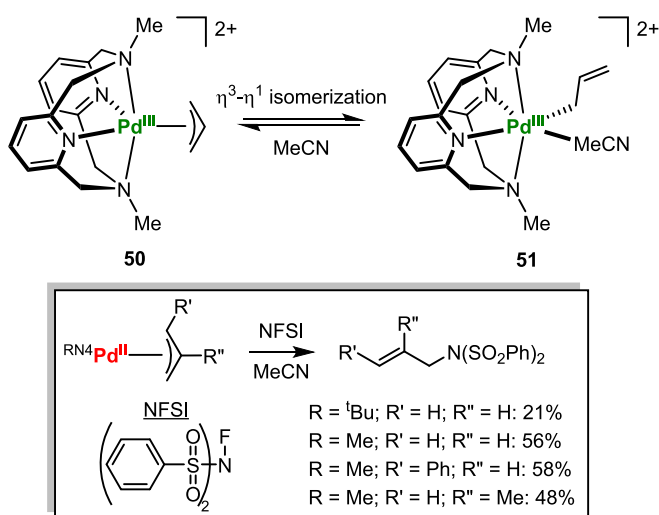


Fig. 24. $(\text{Me}^t\text{BuN}_4)\text{Pd}^{\text{III}}$ -allyl intermediates and their reactivity towards allylic amination.

3.3. Pd^{III} compounds supported by carbanionic, tetradentate $\text{R}^{\text{N}}\text{N}_3\text{C}^-$ ligands

In 2019, Mirica and coworkers synthesized a series of modified pyridinophane ligands where one of the pyridyl groups was replaced

with a *para*-substituted phenyl group, $p\text{-R}^{\text{tBu}}\text{N}_3\text{CH}$ ($\text{R} = \text{H, Me, OMe, CN}$), which were shown to stabilize Pd^{III} and Pd^{IV} complexes. The intriguing feature of these ligands is a $\text{C}_{\text{sp}^2}\text{-H}$ activation process that renders the phenyl group anionic, which aids in the stabilization of high-valent complexes [118]. Such $p\text{-R}^{\text{tBu}}\text{N}_3\text{CH}$ ligands resemble the NCN type pincer ligands, [119] with a pendant pyridine. Interestingly, the Pd^{II} complex **54**, which has a proximal phenyl group does not undergo $\text{C}_{\text{aryl}}\text{-H}$ bond activation on heating or upon the addition of excess acetate to induce a CMD process. However, in presence of CCl_3Br and methyl methacrylate (MMA), which are Kharasch radical addition conditions, C-H bond activation was observed to generate the Pd^{III} complex **55**, which was isolated and characterized (Fig. 26). While the mechanism of this reaction is not immediately obvious, one possibility is the formation of a Pd^{IV} compound, which can undergo comproportionation with **54** to generate **55**. Additionally, $(p\text{-Me}^{\text{tBu}}\text{N}_3\text{C})\text{Pd}^{\text{III}}$ complexes **56** and **57** were obtained by reacting the Pd^{II} analogs with hypervalent iodine reagents such as PhICl_2 , followed by a halide abstraction reaction with thallium salts.

X-ray crystallographic analysis was performed on **56** and a distorted octahedral geometry was found, with Cl and MeCN ligands occupying the equatorial positions, *trans* to the pyridyl N atom and the phenyl C atom, respectively. It is worth mentioning that this is an example of an oxidative $\text{C}_{\text{sp}^2}\text{-H}$ bond activation process to generate a $\text{Pd}^{\text{III}}\text{-C}_{\text{aryl}}$ bond form upon oxidation of the corresponding Pd^{II} complex bearing a unactivated C-H bond. The EPR spectra of these Pd^{III} compounds revealed rhombic signals, consistent with a d_{z^2} ground state, suggesting the metalloradical nature of these compounds despite the presence of a strongly donating carbanion donor. Overall, these results show that the

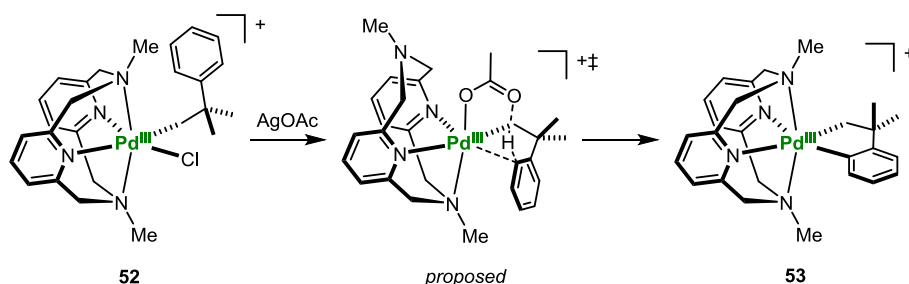


Fig. 25. C-H activation reactivity in a $\text{Me}^{\text{tBu}}\text{N}_4$ -supported Pd^{III} (cyclonophyl) compound via a concerted metalation deprotonation (CMD) pathway.

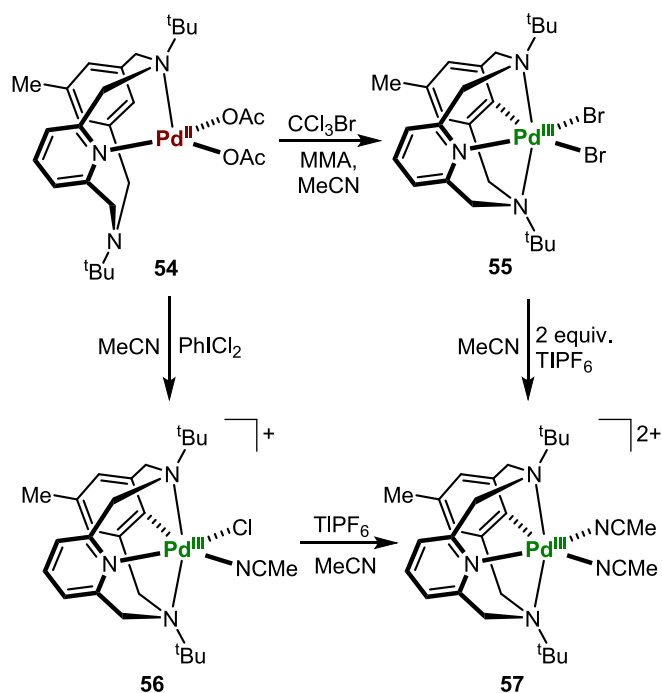


Fig. 26. Syntheses of Pd^{III} complexes supported by the *p*-Me^tBu³N³CH ligand.

RⁿN³CH ligands can stabilize various high-valent Pd complexes. In a recent study, the oxidative addition of a common Pd^I precursor [Pd^I(MeCN)₃]₂(BF₄)₂ with related ligands bearing a C–Br bond in the pyridinophane framework was studied (Fig. 27) [120]. It was found that sterics had a greater effect on reaction rate as compared to electronics, with the N³CB^r ligand bearing neopentyl N-substituents (compounds 59–61) promoting oxidative addition at Pd^I on the order of minutes, while the N³CB^r ligand bearing *t*-butyl N-substituents (compounds 62–64) leading to an oxidative addition on the order of hours, consistent with decreasing favorability of the approach of the Pd^I center.

3.4. Homoleptic Pd^{III} Complexes stabilized by terpyridine

In 2015, Ritter and coworkers unveiled a Pd-catalyzed protocol to synthesize aryl fluorides from arylboronic acids. The reaction was catalyzed by the square planar terpyridine (terpy)-bound Pd^{II}-acetonitrile complex **65** in the presence of Selectfluor and sodium fluoride. To probe the mechanism of the reaction, the authors synthesized a mononuclear, homoleptic Pd^{III} complex **66** stabilized by two terpy ligands by treating the Pd^{II} precursor **65** with terpy, followed by treatment with

one equivalent of Selectfluor (Fig. 28) [121]. X-ray analysis confirmed the Jahn-Teller distorted octahedral geometry of the homoleptic Pd^{III} compound. The EPR spectrum also supports the d⁷ Pd configuration ($g_{av} = 2.09$) with the unpaired electron residing in the d_{z²} orbital, and not on the ligand, which is a possibility for highly conjugated ligands like terpyridine. The Pd^{III} complex was stable in the solid-state under ambient conditions for months and was a competent catalyst in the reaction shown in Fig. 28 in the presence of Selectfluor. This report demonstrates an unusual example of the direct involvement of Pd^{III} in catalysis. Based on kinetic data, an unusual turnover limiting step involving the oxidation of **65** compound by Selectfluor was proposed. This was proposed to form **66** and a Selectfluor radical cation. The latter was proposed to be competent to perform fluoride radical transfer to an aryl trifluoroborate salt to generate a delocalized aryl radical. **66** was then proposed to reduce the aryl radical, generating the fluorinated product, BF₃, and regenerating **65** to close the catalytic cycle.

4. Conclusions

In the present review, we have summarized the strategies developed by various research groups to isolate and characterize mononuclear Pd^I and Pd^{III} coordination complexes, which have broad relevance in inorganic and organometallic chemistry. It is clear that the field is no longer in its infancy from a coordination chemistry perspective. Ligand design principles have emerged that can stabilize and manipulate the reactivity of these compounds. In general, the isolation of Pd^I compounds has relied on conferring kinetic inertness to the metal center to prevent

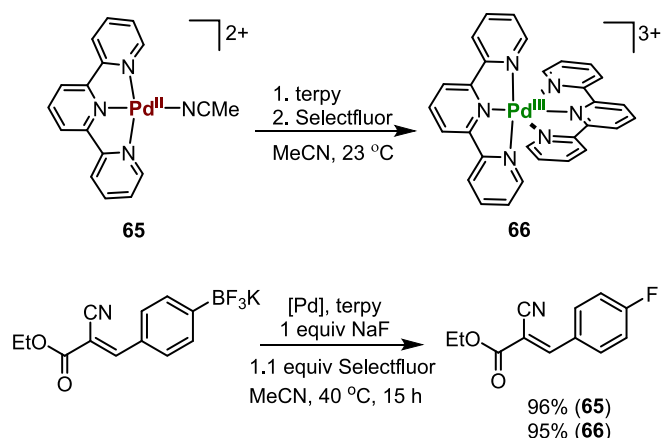


Fig. 28. Synthesis of a homoleptic [(terpy)₂Pd^{III}]³⁺ compound and its catalytic role in the synthesis of aryl fluorides.

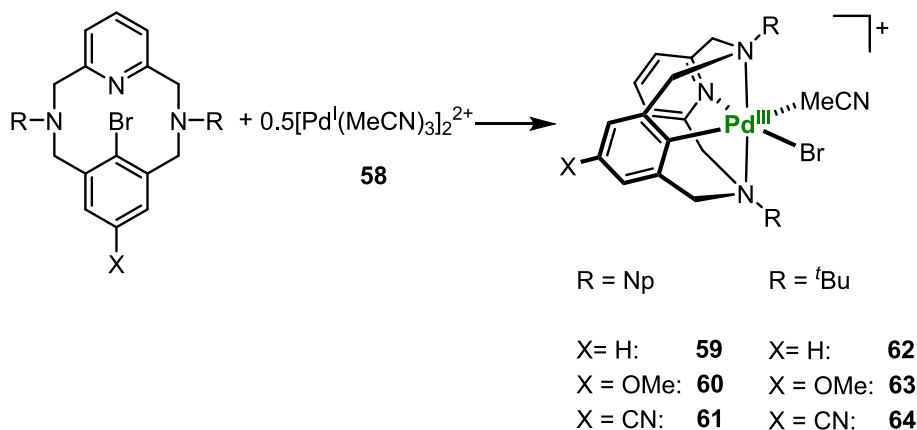


Fig. 27. Oxidative addition of [Pd^I(MeCN)₃]₂²⁺ with modified pyridinophanes containing an aryl bromide.

dimerization. For Pd^{III} compounds, tailoring the ligand field to a distorted octahedral geometry has proved to be the most successful design strategy. However, we believe several unanswered questions remain in the context of the reactivity of these paramagnetic species. The ability to design radical capture strategies at palladium's first-row congener, nickel, has led to tremendous progress in organic chemistry, and much of this has relied on the unique radical reactivity of nickel. At this stage, one must ask the question – can palladium undergo similar one-electron chemistry? We believe that understanding ways to control the reactivity of mononuclear Pd^I and Pd^{III} compounds would lead to the development of new modes of reactivity that diverge from the classical Pd^{0/II} chemistry, and thus expand the reactivity of what is arguably the most catalytically important transition metal in organic chemistry.

CRedit authorship contribution statement

Siddhartha Banerjee: Writing – original draft, Writing – review & editing. **Sagnik Chakrabarti:** Writing – original draft, Writing – review & editing. **Bailey S. Bouley:** Writing – original draft. **Amy J. Wahlmeier:** Writing – original draft. **Liviu M. Mirica:** Funding acquisition, Project administration, Supervision, Writing – review & editing.

Declaration of competing interest

The authors declare that they have no known competing financial interests or personal relationships that could have appeared to influence the work reported in this paper.

Acknowledgements

We thank the National Science Foundation (CHE-2102544 to L. M. M.) for financial support. We would like to dedicate this review to Prof. Harry B. Gray, who has been a great mentor and a towering figure in the field of inorganic chemistry for more than six decades.

Data availability

Data will be made available on request.

References

- [1] C.C. Johansson Seechurn, M.O. Kitching, T.J. Colacot, V. Snieckus, *Angew. Chem. Int. Ed.* 51 (2012) 5062–5085, <https://doi.org/10.1002/anie.201107017>.
- [2] J.G.D. Vries, *Palladium-catalysed coupling reactions, in: Organometallics as Catalysts in the Fine Chemical Industry*, Springer, Berlin, Heidelberg, 2012, pp. 1–34.
- [3] X. Chen, K.M. Engle, D.-H. Wang, J.-Q. Yu, *Angew. Chem. Int. Ed.* 48 (2009) 5094–5115, <https://doi.org/10.1002/anie.200806273>.
- [4] J. He, M. Wasa, K.S.L. Chan, Q. Shao, J.-Q. Yu, *Chem. Rev.* 117 (2017) 8754–8786, <https://doi.org/10.1021/acs.chemrev.6b00622>.
- [5] Z. Li, Z. Wang, N. Chekshin, S. Qian, J.X. Qiao, P.T. Cheng, K.-S. Yeung, W. R. Ewing, J.-Q. Yu, *Science* 372 (2021) 1452–1457, <https://doi.org/10.1126/science.abg2362>.
- [6] N. Kambe, T. Iwasaki, J. Terao, *Chem. Soc. Rev.* 40 (2011) 4937–4947, <https://doi.org/10.1039/c1cs15129k>.
- [7] L.H. Shultz, M. Brookhart, *Organometallics* 20 (2001) 3975–3982, <https://doi.org/10.1021/om010197j>.
- [8] C. Ryan, A.K.D.K. Lewis, S. Caddick, N. Kaltsoyannis, *Theor. Chem. Accounts* 129 (2011) 303–312, <https://doi.org/10.1007/s00214-010-0775-x>.
- [9] Z. Lu, G.C. Fu, *Angew. Chem. Int. Ed.* 49 (2010) 6676–6678, <https://doi.org/10.1002/anie.201003272>.
- [10] L. Griego, J.B. Chae, L.M. Mirica, *Chem* 10 (2024) 867–881, <https://doi.org/10.1016/j.chempr.2023.11.008>.
- [11] J.B. Diccianni, T. Diao, *Trends in Chem.* 1 (2019) 830–844, <https://doi.org/10.1016/j.trechm.2019.08.004>.
- [12] Q. Lin, E.H. Spielvogel, T.N. Diao, *Chem* 9 (2023) 1295–1308, <https://doi.org/10.1016/j.chempr.2023.02.010>.
- [13] T. Iwasaki, N. Kambe, *Top. Curr. Chem.* 374 (2016), <https://doi.org/10.1007/s41061-016-0067-6>.
- [14] L.M. Mirica, J.R. Khusnutdinova, *Coord. Chem. Rev.* 257 (2013) 299–314, <https://doi.org/10.1016/j.ccr.2012.04.030>.
- [15] S. Chakrabarti, S. Sinha, L.M. Mirica, 6.10 - high-valent Pd coordination compounds, in: E.C. Constable, G. Parkin, L. Que Jr. (Eds.), *Comprehensive Coordination Chemistry III*, Elsevier, Oxford, 2021, pp. 375–405, <https://doi.org/10.1016/B978-0-08-102688-5.00105-7>.
- [16] C.R. Work, V.M. Iluc, 6.08 - the coordination chemistry of low-valent nickel, palladium, and platinum, in: E.C. Constable, G. Parkin, L. Que Jr. (Eds.), *Comprehensive Coordination Chemistry III*, Elsevier, Oxford, 2021, pp. 229–347, <https://doi.org/10.1016/B978-0-08-102688-5.00097-0>.
- [17] D.C. Powers, T. Ritter, *Nat. Chem.* 1 (2009) 302–309, <https://doi.org/10.1038/Nchem.246>.
- [18] T. Hama, J.F. Hartwig, *Org. Lett.* 10 (2008) 1545–1548, <https://doi.org/10.1021/ol8002578>.
- [19] C. Fricke, T. Sperger, M. Mendel, F. Schoenebeck, *Angew. Chem. Int. Ed.* 60 (2020) 3355–3366, <https://doi.org/10.1002/anie.202011825>.
- [20] T.J. Colacot, *Platin. Met. Rev.* 53 (2009) 183–188, <https://doi.org/10.1595/147106709X472147>.
- [21] D.C. Powers, T. Ritter, *Top. Organomet. Chem.* 35 (2011) 129–156, https://doi.org/10.1007/978-3-642-17429-2_6.
- [22] K.J. Bonney, F. Proutiere, F. Schoenebeck, *Chem. Sci.* 4 (2013) 4434–4439, <https://doi.org/10.1039/c3sc52054d>.
- [23] G.Y. Yin, I. Kalvet, F. Schoenebeck, *Angew. Chem. Int. Ed.* 54 (2015) 6809–6813, <https://doi.org/10.1002/anie.201501617>.
- [24] D.C. Powers, T. Ritter, *Nat. Chem.* 1 (2009) 302–309, <https://doi.org/10.1038/nchem.246>.
- [25] T. Ishiyama, M. Murata, A. Suzuki, N. Miyaura, *J. Chem. Soc. Chem. Commun.* (1995) 295–296, <https://doi.org/10.1039/C39950000295>.
- [26] G.M. Torres, Y. Liu, B.A. Arndtsen, *Science* 368 (2020) 318–323, <https://doi.org/10.1126/science.aba5901>.
- [27] N. Kvasovs, V. Iziumchenko, V. Palchikov, V. Gevorgyan, *ACS Catal.* 11 (2021) 3749–3754, <https://doi.org/10.1021/acscatal.1c00267>.
- [28] Y. Liu, C. Zhou, M. Jiang, B.A. Arndtsen, *J. Am. Chem. Soc.* 144 (2022) 9413–9420, <https://doi.org/10.1021/jacs.2c01951>.
- [29] S. Sarkar, S. Ghosh, D. Kurandina, Y. Noffel, V. Gevorgyan, *J. Am. Chem. Soc.* 145 (2023) 12224–12232, <https://doi.org/10.1021/jacs.3c02410>.
- [30] N. Kvasovs, J. Fang, F. Kluev, V. Gevorgyan, *J. Am. Chem. Soc.* 145 (2023) 18497–18505, <https://doi.org/10.1021/jacs.3c04968>.
- [31] H. Fang, C. Empel, I. Atodiresi, R.M. Koenigs, *ACS Catal.* 13 (2023) 6445–6451, <https://doi.org/10.1021/acscatal.3c00938>.
- [32] S. Sumino, A. Fusano, T. Fukuyama, I. Ryu, *Acc. Chem. Res.* 47 (2014) 1563–1574, <https://doi.org/10.1021/ar500035q>.
- [33] Q. Liu, X. Dong, J. Li, J. Xiao, Y.H. Dong, H. Liu, *ACS Catal.* 5 (2015) 6111–6137, <https://doi.org/10.1021/acscatal.5b01469>.
- [34] W.-J. Zhou, G.-M. Cao, Z.-P. Zhang, D.-G. Yu, *Chem. Lett.* 48 (2019) 181–191, <https://doi.org/10.1246/cl.190006>.
- [35] P. Chuentragool, D. Kurandina, V. Gevorgyan, *Angew. Chem. Int. Ed.* 58 (2019) 11586–11598, <https://doi.org/10.1002/anie.201813523>.
- [36] X. Sun, X. Dong, H. Liu, Y. Liu, *Adv. Synth. Catal.* 363 (2021) 1527–1558, <https://doi.org/10.1002/adsc.202001315>.
- [37] H.-B. Kraatz, M.E. Van der Boom, Y. Ben-David, D. Milstein, *Isr. J. Chem.* 41 (2001) 163–171, <https://doi.org/10.1560/V0Q8-T3XM-N68W-D8NL>.
- [38] M.P. Lanci, M.S. Remy, W. Kaminsky, J.M. Mayer, M.S. Sanford, *J. Am. Chem. Soc.* 131 (2009) 15618–15620, <https://doi.org/10.1021/ja905816q>.
- [39] G. Manolikakes, P. Knochel, *Angew. Chem. Int. Ed.* 48 (2009) 205–209, <https://doi.org/10.1002/anie.200803730>.
- [40] L. Boisvert, M.C. Denney, H.S. Kloek, K.I. Goldberg, *J. Am. Chem. Soc.* 131 (2009) 15802–15814, <https://doi.org/10.1021/ja9061932>.
- [41] T. Troadec, S.Y. Tan, C.J. Wedge, J.P. Rourke, P.R. Unwin, A.B. Chaplin, *Angew. Chem. Int. Ed.* 55 (2016) 3754–3757, <https://doi.org/10.1002/anie.201511467>.
- [42] C. Dai, G.C. Fu, *J. Am. Chem. Soc.* 123 (2001) 2719–2724, <https://doi.org/10.1021/ja003954y>.
- [43] F. Barrios-Landeros, B.P. Carrow, J.F. Hartwig, *J. Am. Chem. Soc.* 130 (2008) 5842–5843, <https://doi.org/10.1021/ja711159y>.
- [44] M.C. MacInnis, J.C. DeMott, E.M. Zolnhofer, J. Zhou, K. Meyer, R.P. Hughes, O. V. Ozerov, *Chem* 1 (2016) 902–920, <https://doi.org/10.1016/j.chempr.2016.11.007>.
- [45] T.R. O'Toole, J.N. Younathan, B.P. Sullivan, T.J. Meyer, *Inorg. Chem.* 28 (1989) 3923–3926, <https://doi.org/10.1021/ic00319a032>.
- [46] M. Gomberg, *J. Am. Chem. Soc.* 22 (1900) 757–771, <https://doi.org/10.1021/ja02049a006>.
- [47] A.G. Orpen, N.G. Connelly, *Organometallics* 9 (1990) 1206–1210, <https://doi.org/10.1021/om00118a048>.
- [48] B.J. Dunne, R.B. Morris, A.G. Orpen, *J. Chem. Soc. Dalton Trans.* (1991) 653–661, <https://doi.org/10.1039/DT9910000653>.
- [49] H.A. Bent, *Chem. Rev.* 61 (1961) 275–311, <https://doi.org/10.1021/cr60211a005>.
- [50] H.A. Bent, *J. Chem. Phys.* 32 (1960) 1582–1583, <https://doi.org/10.1063/1.1730975>.
- [51] H.A. Bent, *Can. J. Chem.* 38 (1960) 1235–1237, <https://doi.org/10.1139/v60-174>.
- [52] H.A. Bent, *J. Chem. Phys.* 33 (1960) 1259–1260, <https://doi.org/10.1063/1.1731374>.
- [53] H.A. Bent, *J. Chem. Phys.* 33 (1960) 1260–1261, <https://doi.org/10.1063/1.1731375>.
- [54] H.A. Bent, *J. Chem. Educ.* 37 (1960) 616, <https://doi.org/10.1021/ed037p616>.
- [55] H.A. Bent, *J. Chem. Phys.* 33 (1960) 304–305, <https://doi.org/10.1063/1.1731114>.

- [56] T. Krämer, M.R. Gyton, I. Bustos, M.J.G. Sinclair, S.-Y. Tan, C.J. Wedge, S. A. Macgregor, A.B. Chaplin, *J. Am. Chem. Soc.* 145 (2023) 14087–14100, <https://doi.org/10.1021/jacs.3c04167>.
- [57] L. Chen, P. Ren, B.P. Carrow, *J. Am. Chem. Soc.* 138 (2016) 6392–6395, <https://doi.org/10.1021/jacs.6b03215>.
- [58] J.P. Stambuli, M. Bühl, J.F. Hartwig, *J. Am. Chem. Soc.* 124 (2002) 9346–9347, <https://doi.org/10.1021/ja0264394>.
- [59] F. Barrios-Landeros, B.P. Carrow, J.F. Hartwig, *J. Am. Chem. Soc.* 131 (2009) 8141–8154, <https://doi.org/10.1021/ja900798s>.
- [60] M.J.G. Sinclair, A.B. Chaplin, *Dalton Trans.* 51 (2022) 11617–11619, <https://doi.org/10.1039/D2DT02152H>.
- [61] M.J.G. Sinclair, A.B. Chaplin, *Inorg. Chim. Acta* 513 (2020) 119948, <https://doi.org/10.1016/j.ica.2020.119948>.
- [62] Q. Simpson, M.J.G. Sinclair, D.W. Lupton, A.B. Chaplin, J.F. Hooper, *Org. Lett.* 20 (2018) 5537–5540, <https://doi.org/10.1021/acs.orglett.8b01989>.
- [63] C.M. Che, Z.Y. Li, K.Y. Wong, C.K. Poon, T.C.W. Mak, S.M. Peng, *Polyhedron* 13 (1994) 771–776, [https://doi.org/10.1016/S0277-5387\(00\)81683-6](https://doi.org/10.1016/S0277-5387(00)81683-6).
- [64] Y. Meng, Y.R. Gui, P.C. Wu, N.N. Li, M. Zhou, *Russ. J. Coord. Chem.* 37 (2011) 294–301, <https://doi.org/10.1134/S1070328411030079>.
- [65] J. Luo, G.N. Tran, N.P. Rath, L.M. Mirica, *Inorg. Chem.* 59 (2020) 15659–15669, <https://doi.org/10.26434/chemrxiv.12470945.v1>.
- [66] J. Luo, N.P. Rath, L.M. Mirica, *Organometallics* 31 (2013) 3343–3353, <https://doi.org/10.1021/om400286j>.
- [67] S. Chakrabarti, T.J. Woods, L.M. Mirica, *Inorg. Chem.* 62 (2023) 16801–16809, <https://doi.org/10.1021/acs.inorgchem.3c02236>.
- [68] G.N. Tran, B.S. Bouley, L.M. Mirica, *J. Am. Chem. Soc.* 144 (2022) 20008–20015, <https://doi.org/10.1021/jacs.2c08765>.
- [69] S. Chakrabarti, S. Sinha, G.N. Tran, H. Na, L.M. Mirica, *Nat. Commun.* 14 (2023) 905, <https://doi.org/10.1038/s41467-023-36609-7>.
- [70] J. Liu, M.M. Bollmeyer, Y. Kim, D. Xiao, S.N. MacMillan, Q. Chen, X. Leng, S. H. Kim, L. Zhao, K.M. Lancaster, L. Deng, *J. Am. Chem. Soc.* 143 (2021) 10751–10759, <https://doi.org/10.1021/jacs.1c04965>.
- [71] M. Parasram, P. Chuentragool, D. Sarkar, V. Gevorgyan, *J. Am. Chem. Soc.* 138 (2016) 6340–6343, <https://doi.org/10.1021/jacs.6b01628>.
- [72] G.-Z. Wang, R. Shang, W.-M. Cheng, Y. Fu, *J. Am. Chem. Soc.* 139 (2017) 18307–18312, <https://doi.org/10.1021/jacs.7b10009>.
- [73] G.M. Torres, Y. Liu, B.A. Arndtsen, *Science* 368 (2020) 318, <https://doi.org/10.1126/science.aba5901>.
- [74] T. Bruckhoff, J. Ballmann, L.H. Gade, *Angew. Chem. Int. Ed.* (2024) e202320064, <https://doi.org/10.1002/anie.202320064>.
- [75] M. Baya, J. Houghton, D. Konya, Y. Champouret, J.-C. Daran, K.Q. Almeida Leñero, L. Schoon, W.P. Mul, A.B.V. Oort, N. Meijboom, E. Drent, A.G. Orpen, R. Poli, *J. Am. Chem. Soc.* 130 (2008) 10612–10624, <https://doi.org/10.1021/ja8012903>.
- [76] L.S. Merz, C.K. Blasius, H. Wade, L.H. Gade, *Inorg. Chem.* 58 (2019) 6102–6113, <https://doi.org/10.1021/acs.inorgchem.9b00384>.
- [77] C. Yoo, Y. Lee, *Angew. Chem. Int. Ed.* 56 (2017) 9502–9506, <https://doi.org/10.1002/anie.201704487>.
- [78] G. Maties, P. Gómez-Sal, C.G. Yebra, R. Andrés, E. de Jesús, *Inorg. Chem.* 62 (2023) 19838–19842, <https://doi.org/10.1021/acs.inorgchem.3c02878>.
- [79] H.V. Huynh, *Chem. Rev.* 118 (2018) 9457–9492, <https://doi.org/10.1021/acs.chemrev.8b00067>.
- [80] R.A. Kelly III, H. Clavier, S. Giudice, N.M. Scott, E.D. Stevens, J. Bordner, I. Samardjiev, C.D. Hoff, L. Cavallo, S.P. Nolan, *Organometallics* 27 (2008) 202–210, <https://doi.org/10.1021/om701001g>.
- [81] R.J. Rama, M.T. Martín, R. Peloso, M.C. Nicasio, Chapter five - low-coordinate M (0) complexes of group 10 stabilized by phosphorus(III) ligands and N-heterocyclic carbenes, in: P.J. Pérez (Ed.), *Adv. Organomet. Chem.*, Academic Press, 2020, pp. 241–323, <https://doi.org/10.1016/bs.adomc.2020.02.001>.
- [82] M.M. Konnick, I.A. Guzei, S.S. Stahl, *J. Am. Chem. Soc.* 126 (2004) 10212–10213, <https://doi.org/10.1021/ja046884u>.
- [83] X.-C. Cai, S. Majumdar, G.C. Fortman, C.S.J. Cazin, A.M.Z. Slawin, C. Lhermitte, R. Prabhakar, M.E. Germain, T. Palluccio, S.P. Nolan, E.V. Rybak-Akimova, M. Temprado, B. Captain, C.D. Hoff, *J. Am. Chem. Soc.* 133 (2011) 1290–1293, <https://doi.org/10.1021/ja1103348>.
- [84] K. Arentsen, S. Caddick, F.G.N. Cloke, A.P. Herring, P.B. Hitchcock, *Tetrahedron Lett.* 45 (2004) 3511–3515, <https://doi.org/10.1016/j.tetlet.2004.02.134>.
- [85] D.P. Hruszkewycz, J. Wu, N. Hazari, C.D. Incavito, *J. Am. Chem. Soc.* 133 (2011) 3280–3283.
- [86] F.H. Köhler, *Paramagnetic Complexes in Solution: The NMR Approach*, in: *eMagRes*, 2025, <https://doi.org/10.1002/9780470034590.emrstm1229>.
- [87] T. Xia, L. Long, X. Leng, H. Chen, L. Deng, *CS Chem.* 6 (2024) 1–11, <https://doi.org/10.31635/ccschem.024.202404464>.
- [88] A.J. Blake, A.J. Holder, T.I. Hyde, M. Schröder, *J. Chem. Soc. Chem. Commun.* (1987) 987–988, <https://doi.org/10.1039/C39870000987>.
- [89] E. Stephen, A.J. Blake, E. Carter, D. Collison, E.S. Davies, R. Edge, W. Lewis, D. M. Murphy, C. Wilson, R.O. Gould, A.J. Holder, J. McMaster, M. Schröder, *Inorg. Chem.* 51 (2012) 1450–1461, <https://doi.org/10.1021/ic2017006>.
- [90] A.J. Blake, L.M. Gordon, A.J. Holder, T.I. Hyde, G. Reid, M. Schröder, *J. Chem. Soc. Chem. Commun.* (1988) 1452–1454, <https://doi.org/10.1039/C39880001452>.
- [91] J.R. Khusnutdinova, N.P. Rath, L.M. Mirica, *Angew. Chem. Int. Ed.* 50 (2011) 5532–5536, <https://doi.org/10.1002/anie.201100928>.
- [92] J.R. Khusnutdinova, N.P. Rath, L.M. Mirica, *J. Am. Chem. Soc.* 132 (2010) 7303–7305, <https://doi.org/10.1021/ja103001g>.
- [93] J.R. Khusnutdinova, N.P. Rath, L.M. Mirica, *J. Am. Chem. Soc.* 134 (2012) 2414–2422, <https://doi.org/10.1021/ja210841f>.
- [94] F. Tang, S. Park, N.P. Rath, L.M. Mirica, *Dalton Trans.* 47 (2018) 1151–1158, <https://doi.org/10.1039/c7dt04366j>.
- [95] J.R. Khusnutdinova, L.M. Mirica, *Organometallic Pd(III) Complexes in C-C and C-heteroatom bond formation reactions*, in: X. Ribas (Ed.) *C-H and C-X bond functionalization: transition metal mediation*, royal society of chemistry, 2013, pp. 122–158, <https://doi.org/10.1039/9781849737166-00122>.
- [96] F.Z. Tang, F.R. Qu, J.R. Khusnutdinova, N.P. Rath, L.M. Mirica, *Dalton Trans.* 41 (2012) 14046–14050, <https://doi.org/10.1039/c2dt32127k>.
- [97] L.P. Westawker, J.R. Khusnutdinova, R.F. Wallick, L.M. Mirica, *Inorg. Chem.* 62 (2023) 2128–21137, <https://doi.org/10.1021/acs.inorgchem.3c03032>.
- [98] J.R. Khusnutdinova, N.P. Rath, L.M. Mirica, *Inorg. Chem.* 53 (2014) 13112–13129, <https://doi.org/10.1021/ie5023054>.
- [99] J.A. Weil, J.R. Bolton, *Electron Paramagnetic Resonance: Elementary Theory and Practical Applications*, John Wiley & Sons, 2007.
- [100] S. Sinha, L.M. Mirica, *ACS Catal.* 11 (2021) 5202–5211, <https://doi.org/10.1021/acscatal.0c05726>.
- [101] F. Tang, Y. Zhang, N.P. Rath, L.M. Mirica, *Organometallics* 31 (2012) 6690–6696, <https://doi.org/10.1021/om300752w>.
- [102] A.J. Wessel, J.W. Schultz, F. Tang, H. Duan, L.M. Mirica, *Org. Biomol. Chem.* 15 (2017) 9923–9931, <https://doi.org/10.1039/C7OB02508D>.
- [103] J.W. Schultz, N.P. Rath, L.M. Mirica, *Inorg. Chem.* 59 (2020) 11782–11792, <https://doi.org/10.1021/acs.inorgchem.0c01763>.
- [104] B.M. Trost, M.L. Crawley, *Chem. Rev.* 103 (2003) 2921–2944, <https://doi.org/10.1021/cr020027w>.
- [105] B.M. Trost, *J. Organomet. Chem.* 69 (2004) 5813–5837, <https://doi.org/10.1021/jo0491004>.
- [106] L.T. Pilariski, N. Selander, D. Bose, K.J. Szabo, *Org. Lett.* 11 (2009) 5518–5521, <https://doi.org/10.1021/ol9023369>.
- [107] Y.-C. Wang, N.P. Rath, L.M. Mirica, *Organometallics* 41 (2022) 2067–2076, <https://doi.org/10.1021/acs.organomet.2c00215>.
- [108] P.K. Byers, A.J. Canty, *J. Chem. Soc. Chem. Commun.* (1988) 639–641, <https://doi.org/10.1039/C39880000639>.
- [109] D.G. Brown, P.K. Byers, A.J. Canty, *Organometallics* 9 (1990) 1231–1235, <https://doi.org/10.1021/om00118a052>.
- [110] A.J. Canty, H. Jin, A.S. Roberts, B.W. Skelton, P.R. Traill, A.H. White, *Organometallics* 14 (1995) 199–206, <https://doi.org/10.1021/om00001a031>.
- [111] J.W. Schultz, K. Fuchigami, B. Zheng, N.P. Rath, L.M. Mirica, *J. Am. Chem. Soc.* 138 (2016) 12928–12934, <https://doi.org/10.1021/jacs.6b06862>.
- [112] S.M. Smith, O. Planas, L. Gomez, N. Rath, X. Ribas, L.M. Mirica, *Chem. Sci.* 10 (2019) 10366–10372, <https://doi.org/10.1039/c9sc03758f>.
- [113] J. Campora, J.A. Lopez, P. Palma, D. del Rio, E. Carmona, P. Valerga, C. Graiff, A. Tiripicchio, *Inorg. Chem.* 40 (2001) 4116–4126, <https://doi.org/10.1021/ic010114r>.
- [114] B.S. Bouley, F.Z. Tang, D.Y. Bae, L.M. Mirica, *Chem. Sci.* 14 (2023) 3800–3808, <https://doi.org/10.1039/d3sc00034f>.
- [115] J.M. Racowski, N.D. Ball, M.S. Sanford, *J. Am. Chem. Soc.* 133 (2011) 18022–18025, <https://doi.org/10.1021/ja2051099>.
- [116] A. Maleckis, J.W. Kampf, M.S. Sanford, *J. Am. Chem. Soc.* 135 (2013) 6618–6625, <https://doi.org/10.1021/ja401557m>.
- [117] H. Na, A.J. Wessel, S.-T. Kim, M.-H. Baik, L.M. Mirica, *Inorg. Chem. Front.* 11 (2024) 4415–4423, <https://doi.org/10.1039/D4QI01017E>.
- [118] N.P. Ruhs, J. Khusnutdinova, N.P. Rath, L.M. Mirica, *Organometallics* 38 (2019) 3834–3843, <https://doi.org/10.1021/acs.organomet.9b00505>.
- [119] J.-L. Niu, X.-Q. Hao, J.-F. Gong, M.-P. Song, *Dalton Trans.* 40 (2011) 5135–5150, <https://doi.org/10.1039/C0DT01439G>.
- [120] B.S. Bouley, D.Y. Bae, W. Zhou, L. Griego, L.M. Mirica, Submitted ChemRxiv Preprint (2025), <https://doi.org/10.26434/chemrxiv-2024-1b1h3>.
- [121] A.R. Mazzotti, M.G. Campbell, P. Tang, J.M. Murphy, T. Ritter, *J. Am. Chem. Soc.* 135 (2013) 14012–14015, <https://doi.org/10.1021/ja405919z>.